Universität Stuttgart

Geodätisches Institut

GOCE Gravity models and Gravity Gradient Assessment

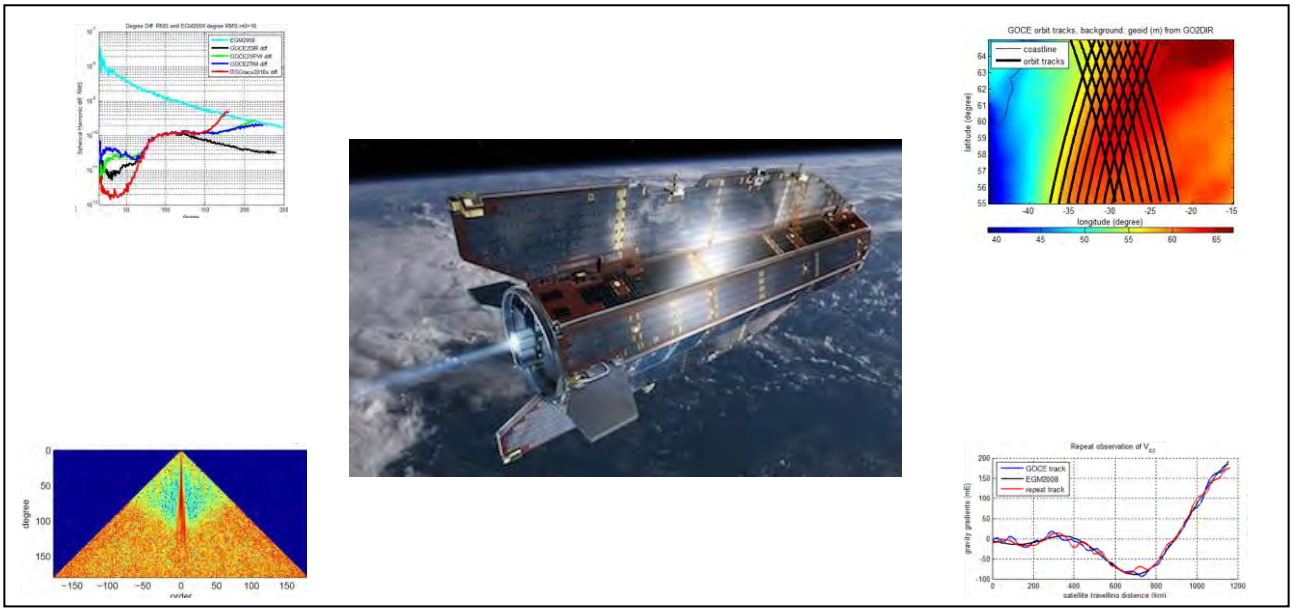

Master thesis

Geomatics Engineering

an der Universität Stuttgart

Lin Wang

Stuttgart, September 2011

Betreuer:

Dr.ir. Wouter van der Wal
Delft University of Technology

Prof. Dr.-Ing. Nico Sneeuw
Universität Stuttgart

Selbstständigkeitserklärung

Hiermit versichere ich, Lin Wang, die vorliegende Arbeit

GOCE Gravity Models and Gravity gradient Assessment

selbständig und unter ausschließlicher Verwendung der angegebenen Literatur und Hilfsmittel erstellt zu haben.

Datum, Ort:_____ Unterschrift: _____

(Lin Wang)

Acknowledgements

The research of this thesis was carried out during a six-month research visit at the Astrodynamics and Space Missions research group in the Faculty of Aerospace Engineering of the Delft University of Technology, the Netherlands. From October 2010 to March 2011, I had the chance to work with this world class researching group. With the good scientific research environment there and the help from my supervisors, I was able to prepare this thesis “GOCE gravity models and gravity gradients assessment”.

First of all, I owe my deepest gratitude to my supervisors, Dr. Wouter van der Wal and Prof. Nico Sneeuw, whose encouragement, guidance and support from the initial to the final level enabled me to develop an understanding of the subject and this thesis. Especially Dr. van der Wal is thanked for his unselfish and unfailing support. His continuous encouragement, patience to answer countless questions and the careful correction for my poor writing skill are the most highly appreciated.

I would like to express my gratitude to Dr. van der Wal, Prof. Sneeuw and Dr. Matthias Weigelt for providing their program of analyzing the spherical harmonic coefficient for this research. I also would like to sincerely thank Dr. P.N.A.M. Visser for the Fortran program and the ASCII format of the GOCE level 2 products. This thesis would not have been possible without all your help.

I sincerely thank Dr. L.L.A Vermeerson and Prof. B.A.C. Ambrosius for offering me this excellent chance to prepare my thesis in Astrodynamics and Space Missions. I also would like to thank all the staff members in Astrodynamics and Space Missions for helpful discussion and great support.

My study aboard was financially supported by the “ERASMUS-Studierendenmobilität” and “Verein Freunde des Studienganges Geodäsie und Geoinformatik an der Universität Stuttgart e.V. ”. I would like to thank those two programs for the support.

Furthermore, I would like to acknowledge the help from my friends for their advice and ideas. Last but not least, I dedicate this thesis to my parents. Without their support, I could not concentrate on my studies.

Abstract

The GOCE (Gravity field and steady-state Ocean Circulation Explorer) mission launched on 17 March 2009 provides for the first time Satellite Gravity Gradiometer (SGG) data. It is designed to recover the Earth gravity anomaly field with an accuracy of better than 1 to 2 mGal with a spatial resolution of 100 km or less. It is necessary to assess the signal and noise in the GOCE data before use.

In this thesis, three GOCE global gravity field models and the gravity gradient observations of level 2 products are assessed with external gravity models and observations.

Three GOCE gravity fields are the sets of spherical harmonics produced by GOCE High level Processing Facility (HPF). They are evaluated in the spectral domain globally and in an area around the Reykjanes Ridge part of the mid-ocean ridge south of Iceland. Three GOCE gravity fields are compared to the global geopotential model EGM2008 and to a state-of-the-art model based only on measurements of the GRACE satellite mission, ITG-Grace2010s. Furthermore ship gravity measurements around the Reykjanes Ridge and a simple parametric geophysical model are used.

Before gravity gradient assessment, a Butterworth band-pass filter was applied to the gradiometer observations at orbit height, because of the 5-100 mHz measurement bandwidth of the GOCE gradiometer. The GOCE gravity gradient measurements of repeat tracks around Reykjanes Ridge are compared after correction from the reference gravity field model (EGM2008).

The outcome of this study will be very helpful for explaining the quality of the GOCE level 2 products which will service in the fields of solid earth physics, oceanography, geodesy and glaciology.

Keywords:

GOCE, satellite gravity gradiometer, Gaussian filter, ship-track measurements, gravity gradient transformation, Butterworth filter, repeat tracks

Table of Contents

List of Tables

List of Figures

Chapter 1. Introduction

1.1 Background

Gravitation is the phenomenon that all physical bodies attract each other with a force proportional to their masses. Earth"s gravitation is the force attracting our body to the Earth. Gravity includes gravitation between a mass and the Earth but also the acceleration due to Earth rotation. As the gravity is influenced by the mass distribution and Earth rotation, measurement of gravity will lead to a better understanding of the density distribution of the Earth.

The name of Isaac Newton comes to mind when we mention gravity and gravitation. An apple falling from a tree helped him get the idea of the *Universal Law of gravitation* more than 300 years ago. Isaac Newton published this research in the book, *Philosophiae naturalis principia mathematica*. He described the gravitational force as being proportional to the individual masses of two attracting bodies and inversely proportional to the square of the distance between each body. It can be described by

$$F_{12} = G\frac{m_1 m_2}{r_{12}^2} \ , \tag{1.1}$$

with F_{12} the gravitational force between object 1 and 2; G the gravitational constant or Newton constant, with a value of $G = 6.672 \cdot 10^{-11}\ \mathrm{m^3 s^{-2} kg^{-1}}$; m_1 and m_2 the masses of object 1 and 2, respectively; r_{12} the distance between the two mass centres of object 1 and 2.

The gravimeter, a tool for measuring gravity, has come in many different forms: pendulums, torsion balances, and static spring gravimeters (Nerem, Jekeli, & Kaula, 1995; Sneeuw, 2006). Before the launch of the first artificial satellite, the Soviet “Sputnik” in 1957, Earth gravity field models were all derived from terrestrial measurements (Jeffreys, 1941). Because of the poor global coverage, the global gravity field models at that time had a poor spatial resolution with much lower accuracy than recently determined gravity field models.

With the improvement of the orbit tracking technology, such as Satellite Laser Ranging (SLR), the orbit of the satellite could be determined more accurately. Using this technique the gravity field could be determined up to a spatial

resolution of 550-1000 km (Marsh et al., 1988; C. Reigber, 1989). The first dedicated gravity mission CHAllenging Mini-satellite Payload (CHAMP) was launched in July 2000 and formed a milestone of gravity field determination by improving gravity and geoid accuracy to 0.5 mGal and 10 cm, respectively, at a spatial resolution of 550 km by only a few month of worth data. This is almost one order of magnitude improvement compared to pre-CHAMP satellite-only models derived from multi-year tracking of some tens of satellites (Ch. Reigber et al., 2003).

A second satellite gravity mission named Gravity Recovery and Climate Experiment (GRACE) made a significant contribution to the gravity field modelling by providing a gravity model with 1 cm geoid accuracy up to degree and order 110 corresponding to about 180 km spatial resolution (Mayer-Guerr, Kurtenbach, & Eicker, 2010).

On March 17, 2009, a third gravity satellite called Gravity Field and Steady-State Ocean Circulation Explorer (GOCE) was launched on a low Earth orbit carrying a highly sensitive gravity gradiometer. Its aim was to determine the static gravity field with a spatial resolution of 100 km with a geoid accuracy of better than 1 cm (ESA, 1999).

1.2 The GOCE mission and GOCE data products

GOCE Mission

The European Space Agency‟s (ESA) first gravity mission, GOCE, is designed to measure gravity gradients with high accuracy, and high spatial resolution, in order to obtain a better static gravity field model. Characteristics from the GOCE satellite mission are shown in Table 1.1 which summarizes information from ESA websites (ESA, 2009, 2010a). The GOCE mission‟s initial life span was about 20 months, but it has been extended by 18 month already. The GOCE mission has taken advantage of an exceptionally long period of low solar activity (ESA, 2011a). Low solar activity results in low density of the thermosphere and makes the drag force on the satellite smaller than expected. This helped GOCE save propellant for a longer orbiting lifetime.

Figure 1.1: GOCE Mission (ESA, 2010c)

Table 1.1: Overview of GOCE (ESA, 2010a)

GOCE	**Mission Overview**
Launch	17 March 2009
Duration	about 38 months, including a three-month commissioning and calibration phase
Orbit	Sun-synchronous, near-circular
– altitude (mean)	about 250 km
– inclination	96.7^{o}
Size	
– length	5 m
– diameter	1 m
Cost	€350 million
Payload	– gradiometer; three pairs of three-axis, servo-controlled, capacitive accelerometers – 12-channel dual-frequency GPS receiver – laser retroreflector enables tracking by ground-base laser

The gradiometer mentioned in Table 1.1 is the most important sensor with six accelerometers in three pairs aligned on three axes as shown in Figure 1.2. From the gradiometer measurements the gravity gradient tensor components can be derived, which contain the second derivatives of the gravity potential. The measurement principle of the gradiometer is measuring the maintaining force between each pair of proof masses of an ensemble of accelerometers. The difference between accelerations measured by each of the two accelerometers in the same direction is the basic differential gradiometric quantity.

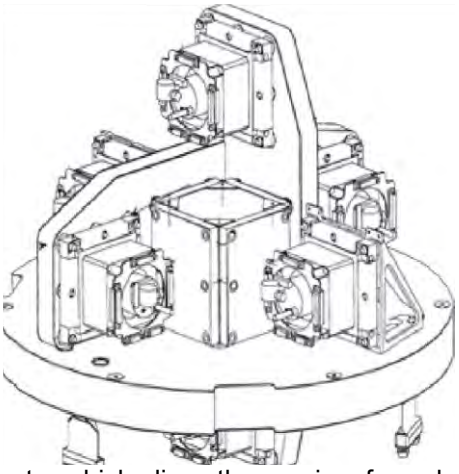

Figure 1.2: GOCE gradiometer which aligns three pairs of accelerometer in three axes with 0.5 m separation for each pair (Rummel & Gruber, 2009)

Mission Objective

The observations and derived gravity models from the GOCE mission will serve science and find application in the fields of solid earth physics, oceanography, geodesy and glaciology (Johannessen et al., 2002; Rummel, Balmino, Johanessen, Visser, & Woodworth, 2002). The pre-launch requirements in Table 1.2 of the GOCE Mission are based on the research requirements for these scientific fields.

For the scientific applications and requirements mentioned in Table 1.2, the GOCE mission has to fulfil the following mission requirements (ESA, 1999):

- Determination of the Earth‟s gravity anomaly field with an accuracy of better than 1 to 2 mGal
- Determination of the geoid with accuracy better than 1 cm in the radial direction
- Spatial resolution of 100 km or less.

Table 1.2 : The requirement in terms of geoid height and gravity anomaly accuracies (ESA, 1999) (rearranged to make the table smaller)

Application	Accuracy		Spatial Resolution (half wavelength – *D* in km)
	Geoid (cm)	Gravity (mGal)	
Solid Earth			
– lithosphere and upper-mantle density structure		1-2	100
– continental lithosphere (sedimentary basins, rifts and tectonic motions)		1-2	20-500
– seismic hazards		1	100
– ocean lithosphere and interaction with asthenosphere		0.5-1	100-200
Oceanography (short-scale)	1-2		100
Ice sheets (rock basement and ice vertical movements)	2	1-5	100-1000
Geodesy			
– levelling by GPS			100-1000
– unification of worldwide height systems	1		100-20 000
– inertial Navigation System	1	~1-5	100-1000
– orbits		~1-3	100-1000
Sea-level change	Many of the above applications, with their specific requirements, are relevant to studies of sea-level change		

Data Products

ESA has defined a ground system, which is in charge of preparing and processing the GOCE observation products. ESA provides data products in different levels derived from the GOCE mission"s observations. The following list provides an overview of each product level (ESA, 2006, 2010b):

- Level 0: time-ordered raw data produced by the instrument and by the platform. This dataset is down-linked during the communication between the satellite and the ground station. The products consist of Satellite-to-Satellite Tracking (SST) data at 1 Hz, six accelerometers at 1 Hz and satellite and instrument ancillary data.
- Level 1a: the instrument time series with the calibration data attached.
- Level 1b: time series along the orbit, including instrument data and other satellite data, such as gravity gradients in the Gradiometer Reference Frame (GRF), frame transformation matrices (rotation quaternions), linear accelerations, angular rates and accelerations, SST measurements and derived positions and reconstructed satellite orbits in the Earth-Fixed Reference Frame and orbit data (position, velocity and time).

- Level 2: this product is generated by the High Level Processing Facility, a distributed system developed and operated by the European GOCE Gravity-Consortium (EGG-C). Level 2 products include three parts: first, pre-processed, externally calibrated, and corrected gravity gradients in both Gradiometer Reference Frame and Terrestrial Reference Frame; second, rapid and precise orbits; third, Gravity field solutions including a variance-covariance matrix and derived quantities (geoid heights, gravity anomalies, and geoid slopes).

In this thesis the Level 2 products are selected for the assessment as they are suitable for the assessment using external reference datasets. Detailed information on the level 2 products is shown in Table 1.3.

Table 1.3: List of GOCE level-2 data products from Level 2 Product Handbook (ESA, 2010b)

Field	Name	Definition
Gravity Gradients	EGG_NOM_2_	Level 2 gravity gradients in Gradiometer Reference Frame with corrections: – Externally calibrated and corrected gravity gradients – Corrections to gravity gradients due to temporal gravity variations – Flags for outliers, fill-in gravity gradients for data gaps with flags – Gravity gradient error estimates
	EGG_TRF_2_	Level 2 gravity gradients in Local North Oriented Frame with corrections. (data component is the same as above)
GOCE Orbits	SST_PSO_2_	Precise science orbits – Reduced-dynamic and kinematic precise science orbits – Rotation matrices between Inertial Reference Frame and Earth Fixed Reference Frame – Variance-covariance information for kinematic positions – Quality report for precise orbits
GOCE Gravity Fields	EGM_GOC_2_	Final GOCE gravity field model – Spherical harmonic series including error estimates – Grids of geoid heights, gravity anomalies and deflections of the vertical – Propagated error estimates in terms of geoid heights – Quality report for GOCE gravity field model
	EGM_GVC_2_	Variance-covariance matrix for the final gravity field in terms of spherical harmonic series
	SST_AUX_2_	Time variable gravity field due to non-tidal mass variations. 6-hourly time series of gravity field spherical harmonic series.

GOCE Gravity Fields (EGM_GOC_2_) contain five gravitational model solutions (until May 5th 2011) presented as a series of spherical harmonic coefficients. There are three gravity field solutions used in this thesis derived from observations in November and December 2009.

There are several time gaps in the Level 2 products because of a software colloquial preventing telemetry of communication and high temperature of the satellite. There is a gap of several weeks for the EGG_NOM product from 6 July 2010 to 6 Oct. 2010. This does not affect our research as the analysis period will be limited from 1 Nov. 2009 to 12 Feb. 2010. There is another data gap from 13 Feb. 2010 to 6 March 2010.

Table 1.4: Main events of GOCE mission after launch (ESA, 2011b)

Time	Milestones since launch
17 March 2009	Launched at 15:21 CET
September 2009	GOCE in measurement mode
29 June 2010	First global gravity model presented at ESA"s Living Planet Symposium
Late July 2010	Software glitch that has rendered the spacecraft unable to send scientific data back to Earth
6 September 2010	GOCE recovers from telemetry glitch preventing the satellite from sending observations to Earth for several weeks
29 September 2010	GOCE resumes normal service
November 2010	GOCE granted 18-month extension

1.3 Motivation

The GOCE mission provides for the first time Satellite Gravity Gradiometer (SGG) data. Implementation of a quality check before using the level 2 data is obviously necessary for understanding the accuracy and stability of the data. It is also important to know the quality of the Level 2 product at ground level and in orbit height.

Observations of the GOCE gradiometer contain stochastic and systematic errors. The systematic error is typically due to misalignment of the accelerometers, scale factor mismatches, and accelerometer varying with time etc. (J. Bouman & Koop, 2003). The stochastic error normally comes from the imperfections of navigation, the discretization error in the analogue-to-digital convertor, signal noise from the instrument etc. The systematic error is usually distributed in the low degrees of the spherical harmonic coefficients while the stochastic error is distributed in the other part.

For understanding the quality of the GOCE gradiometer measurements and the derived gravity field models, it is necessary to separate the analysis into two parts: gravity model assessment and gravity gradient assessment.

Gravity field models assessment

A gravity field model presents the gravity on the Earth surface in terms of spherical harmonic coefficients (see Section 2.1). The GOCE gravity field models used for assessment in this thesis work are three GOCE gravity field model solutions (level 2 product, see Table 1.3). As the gravity field models are mostly (but not completely) based on the GOCE products, the accuracy of the models is meaningful for assessing and validating the GOCE measurement.

In order to assess the GOCE gravity field models, external reference datasets have to be selected. The external reference datasets used here include two global gravity field models, a geophysical model (Turcotte & Schubert, 2002) and ship track observations. One gravity model is a satellite-only model, ITG-Grace2010s (Mayer-Guerr, et al., 2010), from GRACE observations; the other one is a combined gravity model, EGM2008 (Pavlis, A.Holmes, Kenyon, & Factor, 2008), from satellite observations and terrestrial data.

The difference between GOCE solutions and reference gravity models will show either the error in GOCE solutions or the improvement of the GOCE solutions. Low frequency error can be easily detected from a global comparison, but detecting the high frequency error in the spherical harmonic degrees will need regional comparisons.

The area of the mid-Atlantic Ridge (Reykjanes Ridge) south-west of Iceland is the selected region for local comparison as this region is well studied and surveyed, it is a key area for the development of plate tectonic theory. In this research, a geophysical model from Turcotte, et al. (2002) will be used for the comparison at the area of mid-Atlantic Ridge in order to see if the mid-ocean ridge is the main geophysical signal in the gravity field at that location. Ship-track measurements exist in this area and 20 tracks will be selected for the regional comparison in section 3.3.3.

Gravity gradient assessment

The assessment of the satellite gravity gradient (SGG) measured by GOCE gradiometer will show the accuracy of the GOCE gradiometer observations. The external datasets for the assessment are the mentioned gravity fields (ITG-Grace2010s and EGM2008).

Because the reference datasets are gravity fields which represent the gravitational potential on the Earth‟s surface, it will be necessary to transform them to gravity gradients at the satellite orbit in order to compare with the gravity gradient in level 2 product measured by the GOCE gradiometer. The transformation from the Earth surface to the satellite altitude is by so called upward continuation. The result of the upward continued gradients is in the spherical coordinate system, while the level 2 product is in the Gradiometer Reference Frame (GRF) which is a Cartesian coordinate system. In this thesis the only the diagonal elements of the tensor components will be assessed as they are more precise than the other terms. In Section 2.4, Eq. (2.7) to Eq. (2.15) explains that the transformation from spherical coordinates to Cartesian coordinates needs the first derivative terms from spherical harmonic coefficients for gradient in spherical coordinate which are not available for the GOCE gradient measurement obviously. Thus all the comparison for the gradient will be in the Cartesian coordinates system to avoid using the first derivative terms in spherical coordinate.

In this thesis the coordinate system we used for the assessment is the GRF, not the LORF (see section 2.2.3). In section 2.4 we will see that the transformation of the gravity gradient between two Cartesian coordinate system is done by multiplying the rotational matrix and transposed rotational matrix in left and right hand side, respectively. But the accuracy of the gradient components is not at the same level. Therefore the multiplication of the rotational matrix will affect the diagonal components‟ accuracy.

Instead of using the original data of the gravity gradient directly for the comparison with other data, filtering can reduce the error and improve the observation quality. The measurement bandwidth of the gradiometer is 5–100 mHz (ESA, 1999). Because of this bandwidth, the gradients from the gradiometer should be filtered before the comparison. A number of methods for noise filtering are suggested: Bouman (2003) used conservative field characteristics to do along-track interpolation for observation filtering; Cross-over techniques for filtering are presented in (Müller, Jarecki, Wolf, & Brieden, 2010).

The Auto-Regressive-Moving-Average filter and the concept of least-squares for a band limited signal were introduced by Schuh (2003) . Mainly because of time limitation, a conventional Butterworth band-pass filter will be applied to the gradients in this thesis (details in Chapter 4). After applying the band-pass filter, the variation of the SGG along the orbit and between repeat orbits will be discussed in Chapter 4.

In the assessment of the gravity field, Pail et al. (2010) and Gruber et al. (2010) used independent GPS-levelling observations and orbit residuals computed form a number of satellites. Ihde et al. (2010) used gravity data, GPS and levelling control points, astrogeodetic vertical deflections and gravimetric quasigeoid models as terrestrial data sets for external validation of GOCE gravity field models. Hirt et al. (in press) evaluated GOCE static gravity field models via terrestrial gravity, vertical deflections and EGM2008 quasigeoid heights. For the assessment of GOCE gravity gradient, Bouman (2003) and Bouman (2004) used an existing gravity field model to calibrate simulated gradient measurement from the comparison between SGG data and EGM96 derived gradient. The use of local terrestrial gravity data to do the assessment of SGG data over well-surveyed areas was proposed in (Arabelos & Tscherning, 1998), Haagmans et al.(2002), Pail (2002) and Müller et al.(2004); Bouman et al. (2011) analyzed the systematic errors in the computation of gravity gradients; Müller et al. (2010) presented an approach of using cross-overs as an independent relative validation method.

Another validation globally and within a well studied and surveyed area for the newly released GOCE level 2 products will lead to a better understanding of the GOCE observations and GOCE gravity field solutions. GOCE gravity field solutions will compare to a geophysical model for a mid-ocean ridge.

Chapter 2. Gravity and gravity gradient

The previous chapter provides research background, motivation and basic GOCE mission description. In this chapter the mathematical and methodological base are discussed starting from the spherical harmonic representation of the global gravity field and the gravitational models in section 2.1. The relation between gravity and gravity gradient is presented in section 2.3. Coordinate systems and frames mainly used in this thesis as well as the transformations between the different coordinate systems and frames are described in section 2.2. Gravity gradient rotations between different coordinate systems and frames are discussed in section 2.4.

2.1 Gravity field and geopotential models – EGM2008, ITG-Grace2010s and three GOCE solutions

The global gravity field is usually represented in terms of spherical harmonics or ellipsoidal harmonics. In this thesis work, the spherical harmonics representation will be used. The gravitational potential spherical harmonic series is defined in several textbooks(Heiskanen & Moritz, 1967; Moritz, 1989) as

$$\begin{aligned} V(r,\theta,\lambda) &= W(r,\theta,\lambda) - Z(r,\theta,\lambda) \\ &= \frac{GM}{a}\sum_{l=0}^{l_{\max}}\left(\frac{a}{r}\right)^{l+1}\sum_{m=0}^{l}\left(\overline{C}_{lm}\cos m\lambda + \overline{S}_{lm}\sin m\lambda\right)\overline{P}_{lm}(\cos\theta) \end{aligned}, \qquad (2.1)$$

with V gravitational potential at location (r,θ,λ); W gravity potential; Z centrifugal potential; (r,θ,λ) position in polar coordinates, distance to geocenter, co-latitude and longitude of the computation point; GM standard gravitational parameter; l degree of spherical harmonic coefficients; m order of spherical harmonic coefficients; a equatorial radius of the Earth ellipsoid used for the determination of the harmonic coefficients; l_{max} maximum degree of spherical harmonic series; $\overline{P}_{lm}$ normalized Legendre functions of degree l and order m; $\overline{C}_{lm}$, $\overline{S}_{lm}$ Stokes coefficients, cosine and sine term of spherical harmonic coefficients of degree l and order m.

From Eq.(2.1), we can know that with a set of spherical harmonic (SH) series a certain shape of surface can be specified. If this surface is used to describe the

Earth‟s gravity field then it stands for a gravity model. For a better visualization, in the thesis SH coefficients will be presented in an SC format (Sneeuw, 2006) for a better visualization (see Figure 2.1). The SC format places the SH coefficients in the form of a triangle with the sine terms $\overline{S}_{lm}$ on the left side and the cosine terms $\overline{C}_{lm}$ on the other side. The zonal coefficients with order $m = 0$, $\overline{C}_{l0}$, are placed in the centre. The coefficients of the same degree and order $m = l$, $\overline{C}_{ll}$ and $\overline{S}_{ll}$, are called sectorial coefficients are placed on the sides of the triangle. The remaining terms are called tesseral coefficients (Sneeuw, 2006).

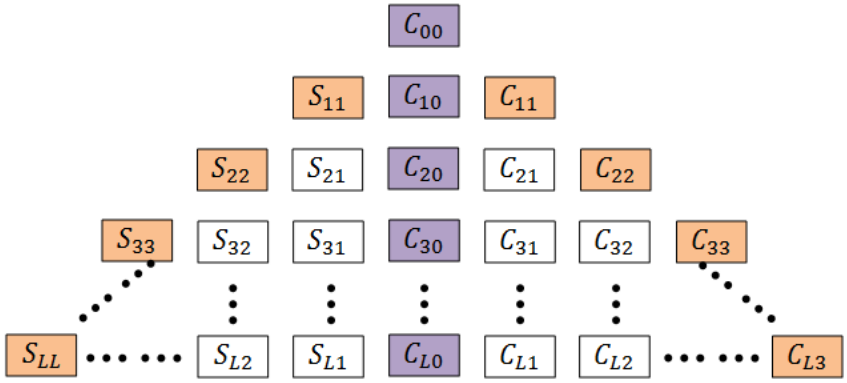

Figure 2.1: SC format for SH coefficients. Blue boxes stand for zonal coefficients, orange boxes stand for sectorial coefficients and the rest are tesseral coefficients

EGM2008

The U.S National Geospatial-Intelligence Agency (NGA) released the Earth Gravitational Model EGM2008 (Pavlis, et al., 2008) which contains coefficients up to maximum spherical harmonic degree 2159 and additional coefficients extending to degree 2190 and order 2159. An overview table of EGM2008 is shown in Table 2.1.

EGM2008 contains observations from terrestrial gravity data and satellite altimetry besides satellite gravity observations. The terrestrial data is not available everywhere, therefore parts of North America, Africa and Asia areas are generated via a “Fill-in” method (Pavlis, et al., 2008).

ITG-Grace2010s

ITG-Grace2010s (Mayer-Guerr, et al., 2010) is a state-of-the-art GRACE-only gravity field model derived from eight years of GRACE mission observations from August 2002 to August 2008. It is the static solution of the ITG-Grace2010 time-

variable gravity field models containing spherical harmonic coefficients up to degree and order 180. Overview information is presented in Table 2.1.

Table 2.1: Overview of EGM2008 and ITG-Grace2010s

	EGM2008	**ITG-Grace2010s**
a (semi-major axis)	6378137.00 m	6378136.6000 m
GM (Standard Gravitational parameter)	$3.986004418 \times 10^{14}\ \mathrm{m^3 s^{-2}}$	$3.9860044150 \times 10^{14}\ \mathrm{m^3 s^{-2}}$
Maximum degree and order	2159 (Additional terms to 2190)	180
Data sources	– Satellite (GRACE) – Altimetry – Terrestrial gravity data	– GRACE observation

From Table 2.1 the most significant difference between the EGM2008 and ITG-Grace2010s is the maximum degree and order. The terrestrial gravity data have much higher spatial resolution than satellite gravity measurement as the observations from satellite mission have a large distance to the Earth"s surface and the satellite tracks are also less dense. However, the satellite gravity observations are globally covering the Earth except for the polar gaps and they have the capacity of measuring the gravity where terrestrial measurements cannot be acquired.

Three GOCE solutions

There are three GOCE gravitational field solutions used in this thesis which are derived from the GOCE Level 2 product data mentioned in section 1.2. These three GOCE gravitational models are generated from the first two-month cycle (from 1 Nov. 2009 to 31 Dec, 2009) of satellite gravity gradient (SGG) observations and satellite-to-satellite tracking (SST). The solutions are: direct solution (Bruinsma et al., 2010), space-wise solution (Migliaccio, Reguzzoni, Sanso, Tscherning, & Veicherts, 2010) and time-wise solution (Pail, Goiginger, Mayrhofer, et al., 2010). These three models will be shortened to DIR, SPW and TIM in figures and tables, respectively.

The direct solution is constructed with prior gravity field information contained in a background reference model. The prior gravity field is EIGEN5C (Foerste, Flechtner, Schmidt, Stubenvoll, & Rothacher, 2008) which is a combination of GRACE, LAGEOS, terrestrial gravimetry and satellite altimetry. The direct

solution is generated from least squares adjustment in the space domain (Pail & Plank, 2002). This method has the capability to transform calibrated and validated SST and SGG observations directly into harmonic coefficients of the gravitational potential field. Detailed information for the direct solution is shown in Table 2.2.

The space-wise solution contains a reference gravitational field of EGM2008 for degree variance modelling and for error calibration of the estimated along-track gravitational potential. The space-wise approach transforms the observations into harmonic coefficients using least-squares collocation in order to connect the discrete observations at different location and altitude to the continuous gravity field, after having transformed the original observations onto a spatial grid (Sünkel, 2001). An overview of the space-wise solution is provided in Table 2.2.

The time-wise solution does not use any gravitational field as a background model or degree variance modelling. The generation approach considers SST and SGG data as a time series. A Fast Fourier Technique is used for transforming the time series of observations into lumped coefficients by several iterations to overcome the error of location for repeat tracks (Sünkel, 2001).

Table 2.2: Overview for direct, space-wise and time-wise solutions model from GOCE first-two-month observation

	Direct solution (DIR)	**Space-wise solution (SPW)**	**Time-wise solution (TIM)**
a (semi-major axis)	6378136.460 m	6378136.300 m	6378136.300 m
GM (Standard Gravitational parameter)	$3.986004415 \times 10^{14}\ \mathrm{m^3 s^{-2}}$	$3.986004415 \times 10^{14}\ \mathrm{m^3 s^{-2}}$	$3.986004415 \times 10^{14}\ \mathrm{m^3 s^{-2}}$
Maximum degree and order	240	210	224
Data sources	Combined data source – GOCE observation (SST, SGG) – A priori model: EGEN5C	Combined data source – GOCE observation (SST, SGG) – EGM2008 used for degree variance modelling and for error calibration	GOCE- only model – GOCE observation (SST, SGG) – without a priori model

From Table 2.2 the most significant difference among these three models are:

Maximum degree and order: The maximum degree and order affect the spatial resolution directly: the direct solution has the highest spatial resolution for the gravity model.

External data source used during the generation: time-wise solution does not rely on any external data source is useful for evaluating the quality of the GOCE satellite observation.

2.2 Coordinate systems

Different datasets can be referred to different coordinate systems and frames. The gradient tensor matrix shown in Eq. (2.16) is in spherical coordinates, but observation such as velocity and position in the level 2 GOCE product are presented in Cartesian coordinates. The transformation between spherical and Cartesian coordinates is shown in Figure 2.2 and Eq. (2.2).

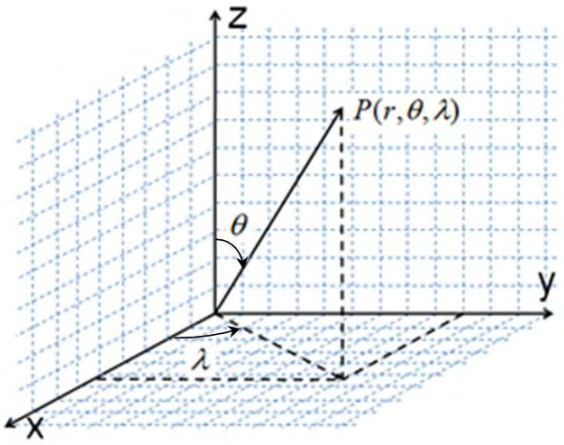

Figure 2.2: Polar and Cartesian coordinates, point P can be presented as (r, θ, λ) or (x, y, z) in polar and Cartesian coordinates, respectively

From Figure 2.2 the Cartesian coordinates (x, y, z) can be expressed in terms of spherical coordinates (r, θ, λ),

$$\begin{cases} x = r\sin\theta\cos\lambda \\ y = r\sin\theta\sin\lambda \\ z = r\cos\theta \end{cases} . \tag{2.2}$$

Several kinds of the coordinate systems and frames exist in this thesis, such as the satellite body frame, earth fixed geocentric coordinate system and inertial geocentric system. They are discussed in the following sections.

2.2.1 Conventional Inertial and Terrestrial Systems (CIS & CTS)

Conventional Inertial and Terrestrial Systems are both geocentric coordinate systems, but the first one is space fixed and the second is the Earth fixed. Newton‟s laws of motion are valid in the Conventional Inertial System (CIS).

CIS is an inertial system for considering and analysing Earth‟s or satellite‟s rotation or movement and it is fixed usually relative to extraterrestrial objects such as stars, quasars, planets or the Moon (Seeber, 2003). The equatorial CIS is shown in Figure 2.3 which is one type of CIS.

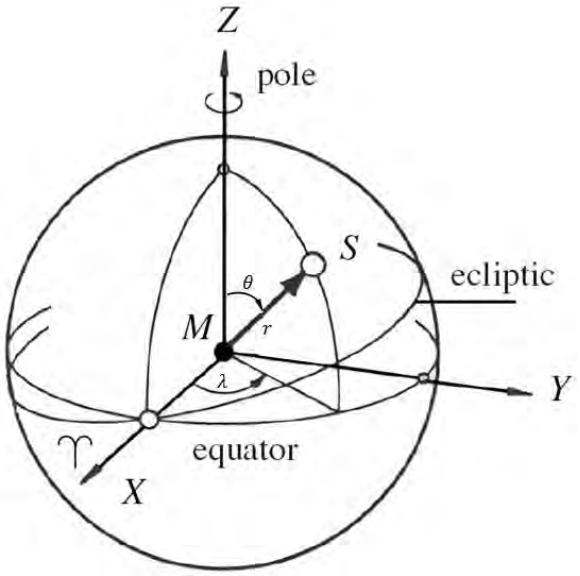

Figure 2.3: Equatorial CIS (Seeber, 2003)

In Figure 2.3, point S can be expressed in spherical coordinates (r,θ,λ) or in Cartesian coordinates (x,y,z), with the X-axis pointing to the first point of Aries Υ, M is geocenter, Z-axis pointing to the North pole at a given epoch T_0, Y-axis is obtained by the right-hand rule.

The Conventional Terrestrial System (CTS) rotates with the Earth and it is a bridge between the CIS and a local coordinate system. A particular form of the CTS can be defined as X-axis points to the crossing point of the mean Greenwich meridian and the true equator, and the Z-axis pointing to the true instantaneous rotation pole of Earth. The Z-axis of the CTS is different from the Z-axis of CIS because of the Earth‟s precession, nutation and polar motion. The transformation between CIS and CTS is shown in Figure 2.4.

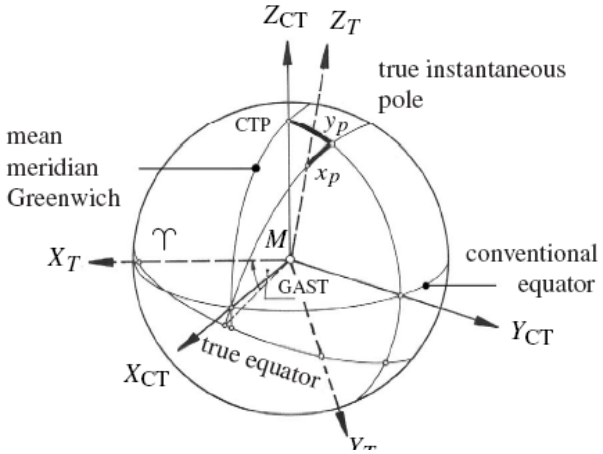

Figure 2.4: CTS and the transformation between CIS and CTS (Seeber, 2003)

In Figure 2.4, (X_T, Y_T, Z_T) are the coordinates in CTS; (X_{CT}, Y_{CT}, Z_{CT}) are the coordinates in CIS; (x_p, y_p) are the pole coordinates difference between Conventional Terrestrial Pole (CTP) and true instantaneous pole. Greenwich Sidereal Time (GAST) is the angle between CIS and CTS for the relative rotation of X_{CT}-axis. The transformation matrix $\mathbf{R}$ for the coordinate transformation from CIS to CTS (Seeber, 2003),

$$\begin{aligned}\mathbf{R} &= \mathbf{R}_2(-x_p)\mathbf{R}_1(-y_p)\mathbf{R}_3(\mathrm{GAST}) \\ &= \begin{pmatrix} 1 & 0 & x_p \\ 0 & 1 & 0 \\ x_p & 0 & 1 \end{pmatrix}\begin{pmatrix} 1 & 0 & 0 \\ 0 & 1 & -y_p \\ 0 & y_p & 1 \end{pmatrix}\begin{pmatrix} \cos(\mathrm{GAST}) & \sin(\mathrm{GAST}) & 0 \\ -\sin(\mathrm{GAST}) & \cos(\mathrm{GAST}) & 0 \\ 0 & 0 & 1 \end{pmatrix},\end{aligned} \tag{2.3}$$

with $\mathbf{R}_1$, $\mathbf{R}_2$, $\mathbf{R}_3$ the transformation matrixes for rotation around X-axis, Y-axis and Z-axis, respectively.

2.2.2 Gradiometer Reference Frame (GRF)

The gravity gradient tensor measured by the gradiometer of GOCE is in the Gradiometer Reference Frame (GRF). The gradiometer contains six accelerometers aligned in three axes which define the GRF. Each pair of accelerometers fixes one axis of the GRF (see Figure 2.5).

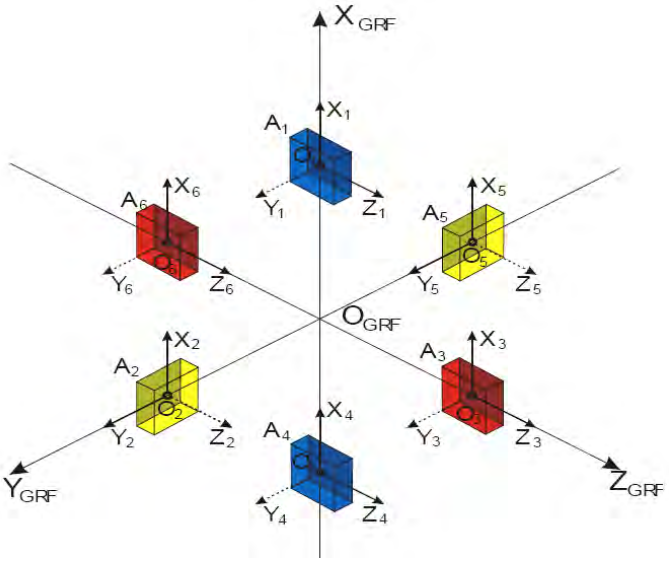

Figure 2.5: Definition of GRF and the six accelerometers (ESA, 2010b)

In Figure 2.5, $(X_{GRF}, Y_{GRF}, Z_{GRF})$ are the three GRF axes; each cuboid $(A_1, A_2, \ldots\ldots, A_6)$ stands for an accelerometer. (X_i, Y_i, Z_i) with $i = 1,2 \ldots\ldots 6$ are the accelerometer reference frames for the six accelerameters. Each accelerometer in GOCE is not sensitive to acceleration in each of the three axes in the accelerometer reference frame. Solid lines are the sensitive axes and dashed lines are the less sensitive axes.

2.2.3 Local Orbital Reference Frame (LORF)

GRF is a frame derived from the gradiometer and it is one type of platform coordinate frame. The LORF is another one, derived from the satellite body. The centre of LORF is the actual mass centre of the satellite. The X -axis is the direction of the GOCE velocity, Y -axis is perpendicular to the orbit surface (the same direction as the orbital angular momentum) and Z -axis is fixed by the right-hand rule. The definition of LORF and the relation between GRF is shown in Figure 2.6.

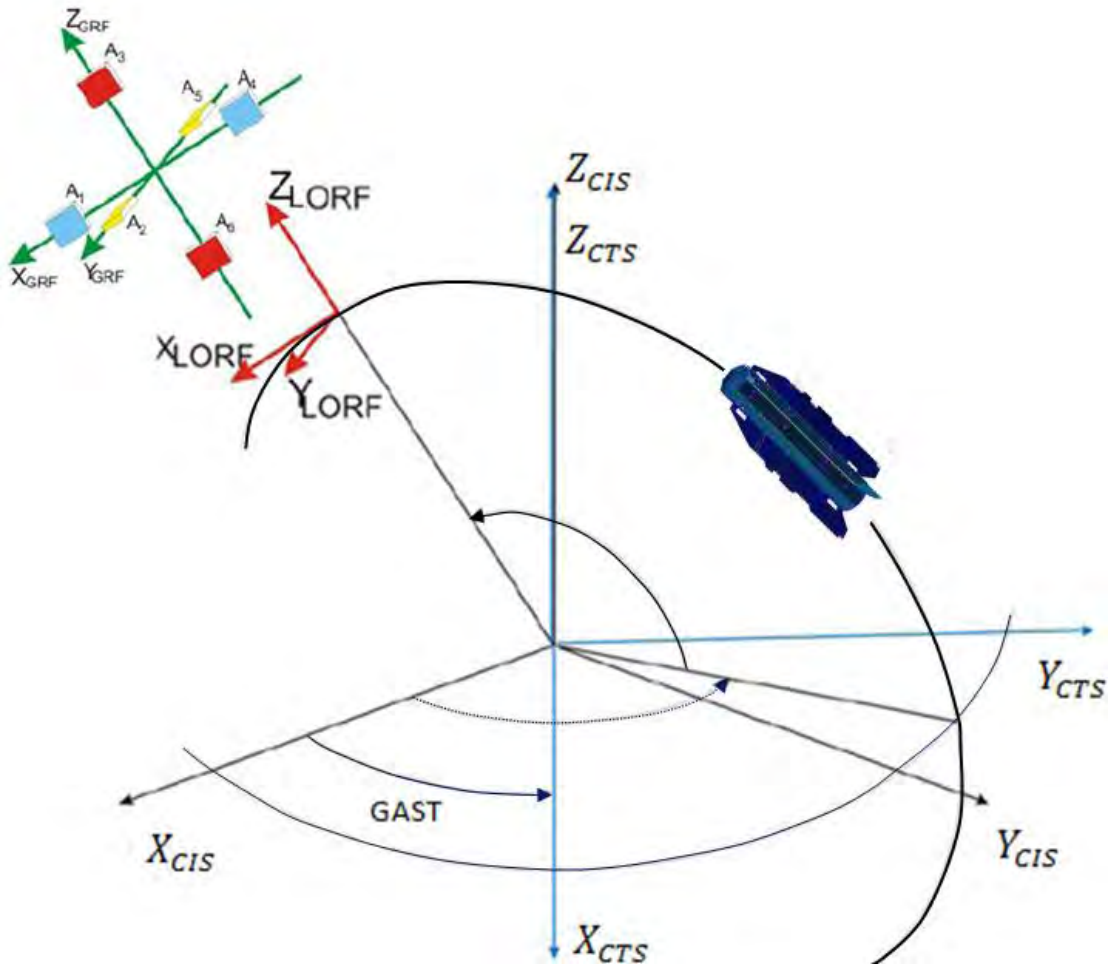

Figure 2.6: Definition of LORF and the relation between LORF and GRF (ESA, 2010b)

Figure 2.6 shows that the GRF does not fully coincide with the LORF due to the existence of tiny misalignments and the constant bias.

2.3 Gravity gradients derived from geopotential models

The gravity gradient is the gravity change between two infinitely close points devides by the coordinates in a certain direction, and it is the second derivative of geopotential. A gravitational model presentation in spherical harmonics at the Earth"s surface yields the corresponding gravity gradient at orbit height by upward continuation.

From Eq. (2.1) the first derivatives of geopotential are

$$V_r = -\frac{GM}{a^2}\sum_{l=0}^{l_{\max}}(l+1)\left(\frac{a}{r}\right)^{l+2}\sum_{m=0}^{l}\left(\overline{C}_{lm}\cos m\lambda + \overline{S}_{lm}\sin m\lambda\right)\overline{P}_{lm}(\cos\theta)\ , \qquad (2.4)$$

$$V_\theta = -\frac{GM}{a}\sum_{l=0}^{l_{\max}}\left(\frac{a}{r}\right)^{l+1}\sum_{m=0}^{l}\left(\overline{C}_{lm}\cos m\lambda + \overline{S}_{lm}\sin m\lambda\right)\overline{P}_{lm}^{(1)}(\cos\theta)\sin(\theta)\ , \qquad (2.5)$$

$$V_\lambda = \frac{GM}{a}\sum_{l=0}^{l_{\max}}\left(\frac{a}{r}\right)^{l+1}\sum_{m=0}^{l} m\left(-\overline{C}_{lm}\sin m\lambda + \overline{S}_{lm}\cos m\lambda\right)\overline{P}_{lm}(\cos\theta)\ , \qquad (2.6)$$

where V_r, V_θ and V_λ are first derivative of geopotential w.r.t. radius, co-latitude, longitude for a certain location, the subscript stand for the partial derivative. $\overline{P_{lm}^{(i)}}$ is the i-th derivative of the normalized Legendre functions.

The solution for the derivative of normalized Legendre polynomials is mentioned by Ilk (1983). Continue the derivatives for Eqs. (2.4), (2.5) and (2.6) yielding the second derivatives (Novák & Grafarend, 2006),

$$V_{rr} = \frac{GM}{a^3}\sum_{l=0}^{l_{\max}}(l+1)(l+2)\left(\frac{a}{r}\right)^{l+3}\sum_{m=0}^{l}\left(\overline{C}_{lm}\cos m\lambda + \overline{S}_{lm}\sin m\lambda\right)\overline{P}_{lm}(\cos\theta)\ , \qquad (2.7)$$

$$V_{r\theta} = \frac{GM}{a^2}\sum_{l=0}^{l_{\max}}(l+1)\left(\frac{a}{r}\right)^{l+2}\sum_{m=0}^{l}\left(\overline{C}_{lm}\cos m\lambda + \overline{S}_{lm}\sin m\lambda\right)\overline{P}_{lm}^{(1)}(\cos\theta)\sin\theta\ , \qquad (2.8)$$

$$V_{r\lambda} = -\frac{GM}{a^2}\sum_{l=0}^{l_{\max}}(l+1)\left(\frac{a}{r}\right)^{l+2}\sum_{m=0}^{l} m\left(-\overline{C}_{lm}\sin m\lambda + \overline{S}_{lm}\cos m\lambda\right)\overline{P}_{lm}(\cos\theta)\ , \qquad (2.9)$$

$$V_{\theta r} = V_{r\theta}\ , \qquad (2.10)$$

$$V_{\theta\theta} = -\frac{GM}{a}\sum_{l=0}^{l_{\max}}\left(\frac{a}{r}\right)^{l+1}\sum_{m=0}^{l}\left(\overline{C}_{lm}\cos m\lambda + \overline{S}_{lm}\sin m\lambda\right)\left(-\overline{P}_{lm}^{(2)}(\cos\theta)\sin^2(\theta) + \overline{P}_{lm}^{(1)}(\cos\theta)\cos(\theta)\right)\ , \qquad (2.11)$$

$$V_{\theta\lambda} = -\frac{GM}{a}\sum_{l=0}^{l_{\max}}\left(\frac{a}{r}\right)^{l+1}\sum_{m=0}^{l} m\left(-\overline{C}_{lm}\sin m\lambda + \overline{S}_{lm}\cos m\lambda\right)\overline{P}_{lm}^{(1)}(\cos\theta)\sin(\theta)\ , \qquad (2.12)$$

$$V_{\lambda r} = V_{r\lambda}\ , \qquad (2.13)$$

$$V_{\lambda\theta} = V_{\theta\lambda}\ , \qquad (2.14)$$

$$V_{\lambda\lambda} = -\frac{GM}{a}\sum_{l=0}^{l_{\max}}\left(\frac{a}{r}\right)^{l+1}\sum_{m=0}^{l} m^2(\overline{C}_{lm}\cos m\lambda + \overline{S}_{lm}\sin m\lambda)\overline{P}_{lm}(\cos\theta)\ . \qquad (2.15)$$

From the nine equations above, the second geopotential derivatives can be presented in terms of spherical harmonics. Full geopotential gradient tensor

$\nabla\nabla V$ at the point $P(r,\theta,\lambda)$ in the spherical coordinate $x^p \in (r,\theta,\lambda)$ is expressed in (Casotto & Fantino, 2009) as:

$$\nabla\nabla V = \begin{pmatrix} V^*_{rr} & V^*_{\theta r} & V^*_{\lambda r} \\ V^*_{\theta r} & V^*_{\theta\theta} & V^*_{\theta\lambda} \\ V^*_{\lambda r} & V^*_{\theta\lambda} & V^*_{\lambda\lambda} \end{pmatrix}$$

$$= \begin{pmatrix} V_{rr} & \frac{1}{r}\left(V_{\theta r} - \frac{V_\lambda}{r}\right) & \frac{1}{r\sin\theta}\left(V_{\lambda r} - \frac{V_\lambda}{r}\right) \\ \frac{1}{r}\left(V_{\theta r} - \frac{V_\lambda}{r}\right) & \frac{1}{r}\left(\frac{V_{\theta\theta}}{r} + V_r\right) & \frac{1}{r^2\sin\theta}V_{\theta\lambda} \\ \frac{1}{r\sin\theta}\left(V_{\lambda r} - \frac{V_\lambda}{r}\right) & \frac{1}{r^2\sin\theta}V_{\lambda\theta} & \frac{V_{\lambda\lambda}}{r^2\sin^2\theta} + \frac{V_r}{r} - \frac{V_\theta}{r^2\tan\theta} \end{pmatrix}, \quad (2.16)$$

with the subscription * denote the tensor component, not the second derivative terms.

According the Eq. (2.7) to (2.16), $\nabla\nabla V$ can be expressed by the spherical harmonic coefficients.

2.4 Gravity gradient rotation and transformation

In the Chapter 4 for the gradient comparison, the gravity gradient generated from the model in terms of SH coefficients is in the spherical coordinate system, but the measured gradients from the GOCE gradiometer are in the GRF which is a Cartesian coordinate. The transformation equations for the potential derivatives are presented in (Koop & Stelpstra, 1989) as

$$V_x = -\frac{1}{r}V_\theta \quad , \quad (2.17)$$

$$V_y = \frac{1}{r\sin\theta}V_\lambda \quad , \quad (2.18)$$

$$V_z = V_r \quad , \quad (2.19)$$

$$V_{xx} = \frac{1}{r}V_r + \frac{1}{r^2}V_{\theta\theta} \quad , \quad (2.20)$$

$$V_{xy} = \frac{\cos\theta}{r^2\sin^2\theta}V_\lambda - \frac{1}{r^2\sin\theta}V_{\lambda\theta} \quad , \quad (2.21)$$

$$V_{xz} = \frac{1}{r^2} V_\theta - \frac{1}{r} V_{r\theta} \quad , \tag{2.22}$$

$$V_{yy} = \frac{1}{r} V_r + \frac{1}{r^2 \tan\theta} V_\theta + \frac{1}{r^2 \sin\theta} V_{\lambda\lambda} \quad , \tag{2.23}$$

$$V_{yz} = \frac{1}{r \sin\theta} V_{r\lambda} - \frac{1}{r^2 \sin\theta} V_\lambda \quad , \tag{2.24}$$

$$V_{zz} = V_{rr} \quad , \tag{2.25}$$

where $x^q = (x, y, z)$ is in GRF and $x^p = (r, \theta, \lambda)$ is in spherical coordinate.

The second order derivatives of gravity potential in Cartesian coordinate equals to the gradient tensor component. The transformation equations from the gradient tensor components in spherical coordinates to the Cartesian coordinate are presented in (Casotto & Fantino, 2009) written as

$$V_x = -V_\lambda^* \sin\lambda - V_\theta^* \cos\theta\cos\lambda + V_r^* \sin\theta\cos\lambda \quad , \tag{2.26}$$

$$V_y = V_\lambda^* \cos\lambda - V_\theta^* \cos\theta\sin\lambda + V_r^* \sin\theta\sin\lambda \quad , \tag{2.27}$$

$$V_z = V_\theta^* \sin\theta + V_r^* \cos\theta \quad , \tag{2.28}$$

$$\begin{aligned} V_{xx} = {} & V_{\lambda\lambda}^* \sin^2\lambda + V_{\lambda\theta}^* \cos\theta \sin 2\lambda - V_{\lambda r}^* \sin\theta \sin 2\lambda \\ & + V_{\theta\theta}^* \sin^2\theta\cos^2\lambda - 2V_{\theta r}^* \sin\theta\cos\theta\cos^2\lambda + V_{rr}^* \sin^2\theta\cos^2\lambda \end{aligned} \quad , \tag{2.29}$$

$$\begin{aligned} V_{xy} = {} & -V_{\lambda\lambda}^* \cos\lambda\sin\lambda - V_{\lambda\theta}^* \cos\theta\cos 2\lambda + V_{\lambda r}^* \sin\theta\cos 2\lambda \\ & + V_{\theta\theta}^* \cos^2\theta\cos\lambda\sin\lambda - V_{\theta r}^* \sin 2\theta\cos\lambda\sin\lambda + V_{rr}^* \sin^2\theta\cos\lambda\sin\lambda \end{aligned} \quad , \tag{2.30}$$

$$\begin{aligned} V_{xz} = {} & -V_{\lambda\theta}^* \sin\theta\sin\lambda - V_{\lambda r}^* \cos\theta\sin\lambda - V_{\theta\theta}^* \sin\theta\cos\theta\cos\lambda \\ & - V_{\theta r}^* \cos 2\theta\cos\lambda\sin\lambda + V_{rr}^* \sin^2\theta\cos\lambda\sin\lambda \end{aligned} \quad , \tag{2.31}$$

$$\begin{aligned} V_{yy} = {} & V_{\lambda\lambda}^* \cos^2\lambda\sin\lambda - V_{\lambda\theta}^* \cos\theta\sin 2\lambda + V_{\lambda r}^* \sin\theta\sin 2\lambda \\ & + V_{\theta\theta}^* \cos^2\theta\sin^2\lambda - V_{\theta r}^* \sin\theta\cos\theta\sin 2\lambda + V_{rr}^* \sin^2\theta\sin^2\lambda \end{aligned} \quad , \tag{2.32}$$

$$\begin{aligned} V_{xy} = {} & V_{\lambda\theta}^* \sin\theta\cos\lambda + V_{\lambda r}^* \cos\theta\cos\lambda - V_{\theta\theta}^* \sin\theta\cos\theta\sin\lambda \\ & - V_{\theta r}^* \cos 2\theta\sin\lambda + V_{rr}^* \sin\theta\cos\theta\sin\lambda \end{aligned} \quad , \tag{2.33}$$

$$\begin{aligned} V_{yz} = {} & V_{\lambda\theta}^* \sin\theta\cos\lambda + V_{\lambda r}^* \cos\theta\cos\lambda - V_{\theta\theta}^* \sin\theta\cos\theta\sin\lambda \\ & - V_{\theta r}^* \cos 2\theta\sin\lambda\sin\lambda + V_{rr}^* \sin\theta\cos\theta\sin\lambda \end{aligned} \quad , \tag{2.34}$$

$$V_{zz} = V_{\theta\theta}^* \sin^2\theta + V_{\theta r}^* \sin 2\theta + V_{rr}^* \cos^2\theta \, , \tag{2.35}$$

where the subscription * denotes the gradient term, not the derivatives. In Cartesian coordinates, derivative terms equal to the corresponding gradient terms, $V_{x_i^q x_j^q} = V^*_{x_i^q x_j^q}$ with $i, j \in (1,2,3)$ and $\left(x_1^q, x_2^q, x_3^q\right) = (x, y, z)$.

The transformation equation of gradient tensor matrices between two Cartesian coordinate $x^{q_1} = (x_1, y_1, z_1)$ and $x^{q_2} = (x_2, y_2, z_2)$ can be derived from the chain rule of partial derivatives (Tscherning, 1976) and it obtains

$$\nabla\nabla V^{x^{q_1}} = \mathbf{R} \bullet \nabla\nabla V^{x^{q_2}} \bullet \mathbf{R}^T \ , \tag{2.36}$$

with $\mathbf{R}$ the rotational matrix between two Cartesian coordinates.

Chapter 3. GOCE gravity models assessment

The former chapter provides a basic theory background for this thesis. In this chapter, three GOCE gravity models will be assessed in the spectral domain and the spatial domain, for both a global area and a local area. Comparison will be limited up to degree and order 180 as the maximal degree of ITG-Grace2010s is 180.

In section 3.1, the result of the comparison in the spectral domain will be discussed for the spherical harmonic coefficients of the reference models ITG-Grace2010s and EGM2008. Comparison in the spatial domain for global area is introduced in section 3.2.

In Section 3.3, we select the mid-oceanic ridge (Reykjanes Ridge) south-west of Iceland for local comparison was explained in Section 1.3. GOCE gravity field solutions are compared to a geophysical model, EGM2008 and ship track gravity measurements.

The gravity models derived from GOCE have been used and assessed in serveral publications. Bingham, et al. (2011) presented an improvement that the estimate of the North Atlantic"s ocean circulation from a two month GOCE model is superior to an estimate from ITG-Grace2010s based on 8 years of GRACE data. Pail, et al. (2010) found lower RMS of geoid height differences comparing to regional GPS/Levelling observations for the GOCE-GRACE combined model (GOCO01S) and GOCE-only model (GOCE time-wise solution). The aim of this chapter is to detect whether any improvement can be found in GOCE gravity field solutions.

3.1 Spherical harmonic coefficients comparison

It is showed in Figure 3.1 that the procedure of comparing spherical harmonic (SH) coefficients after subtracting a reference model for all GOCE solutions (DIR, SPW and TIM) and the GRACE gravity model (ITG-Grace2010s). The differences are shown in Figure 3.2.

From the result in Figure 3.2, the difference between space-wise solution and time-wise solution appears a pattern for low order terms ($m \leq 15$). These are

called near-zonal coefficients in this thesis. Near-zonal coefficients are affected by the polar gaps of 6.5 degree latitude as no observations are available near the poles due to the inclination of about 96.5 degree. More information about the effect of the polar gap can be found in (Sneeuw & van Gelderen, 1997). The low degrees ($l \leq 100$) differences of three GOCE solutions are larger than those of ITG-Grace2010s. This is due to EGM2008 containing the observations from GRACE mission. The high degree ($l \geq 160$) coefficients from the GOCE solutions are closer to EGM2008 than ITG-Grace2010s.

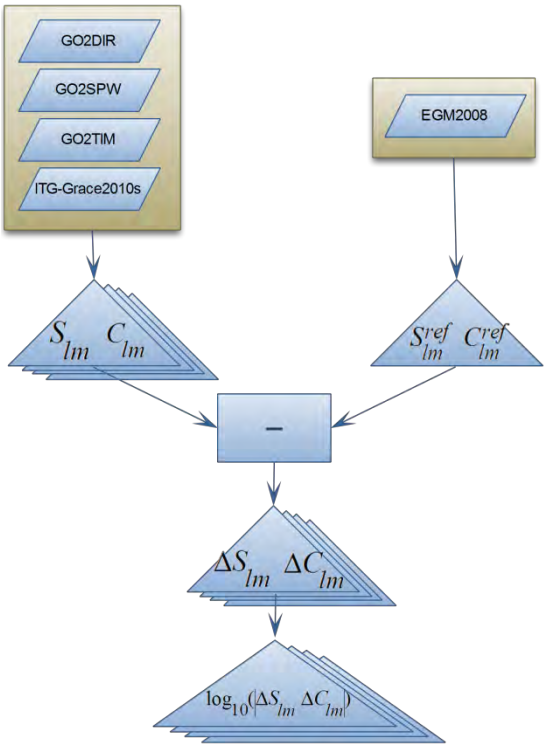

Figure 3.1: Procedure of spherical harmonic coefficient comparison of the subtraction to reference model (EGM2008)

Spherical harmonic degree RMS, RMS_l, shows the magnitude of the SH coefficients and it is plotted in Figure 3.3 and Figure 3.4 as background. RMS_l can be written as

$$\mathrm{RMS}_l = \sqrt{\frac{\sum_0^l \left(C_{lm}{}^2 + S_{lm}{}^2\right)}{2l+1}}, \tag{3.1}$$

with RMS_l SH degree RMS; (l, m) degree and order for SH coefficients; (C_{lm}, S_{lm}) SH coefficients.

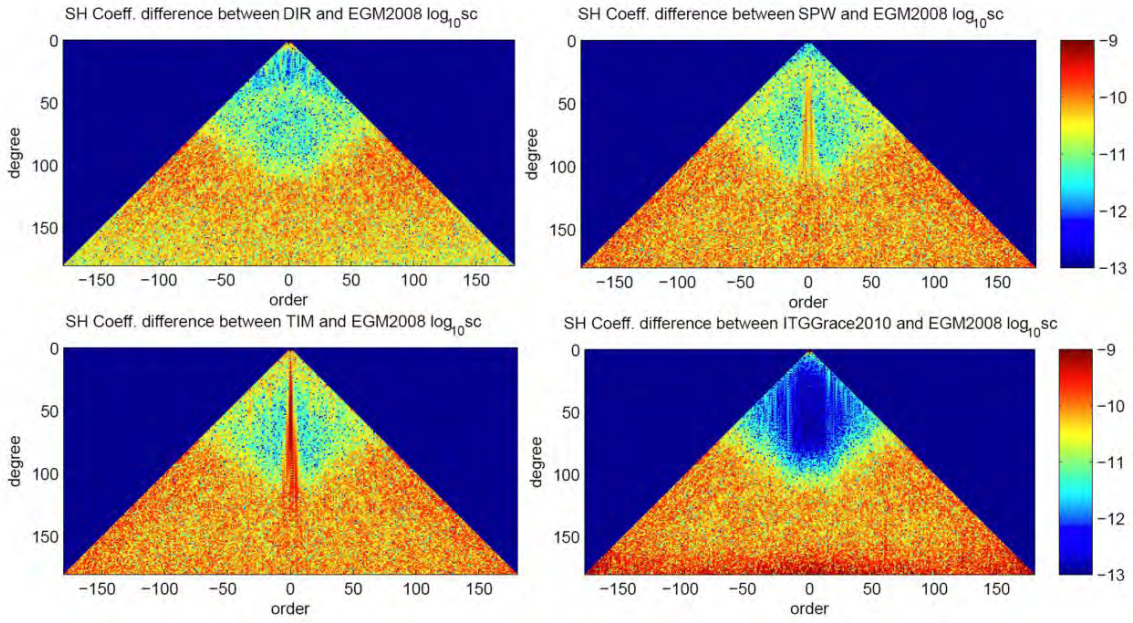

Figure 3.2: Spherical harmonic coefficient difference w.r.t. EGM2008, shown in logarithm

The lower order part of the spherical harmonics is affected by the polar gap. In order to minimize the impact of the polar gaps, the near zonal coefficients are omitted for orders smaller than 16. The omitted degree RMS ($\Delta\mathrm{RMS}_l$, see Eq. (3.2)) with respect to reference models (EGM2008 or ITG-Grace2010s) is computed for the comparison in spectral domain from three GOCE solutions and an external gravity model (ITG-Grace2010s or EGM2008).

$$\Delta\mathrm{RMS}_l = \sqrt{\frac{\sum_{m=m_0}^{l}\left(\Delta C_{lm}{}^2 + \Delta S_{lm}{}^2\right)}{2(l-m_0+1)}}\,, \tag{3.2}$$

where $\Delta\mathrm{RMS}_l$ is RMS for degree l of the subtracted SH coefficients with respect to reference models; (ΔC_{lm}, ΔS_{lm}) are SH coefficients with respect to reference models and m_0 is the start order of computation, orders $m < m_0$ are eliminated.

The results of the $\Delta\mathrm{RMS}_l$ with full order and $m_0 = 16$ is shown in Figure 3.3. In the left figure, the GOCE time-wise solution is oscillating because of the polar gaps. After the elimination of the low order terms, the effect is mainly removed, similar to the small oscillation in the space-wise solution for degrees 50 to 70. It is obvious that the three GOCE solutions do not perform as well as ITG-Grace2010s for degree smaller than 70, but for the high degree terms (≥ 150 for space-wise and time-wise solutions, ≥ 120 for direct solution) the three GOCE solutions perform better than ITG-Grace2010s. The $\Delta\mathrm{RMS}_l$ of the ITG-Grace2010s shows the growing error for degrees larger than 150. Especially for degrees over 170 where the $\Delta\mathrm{RMS}_l$ is even larger than the RMS_l of

EGM2008. Between the degrees of 70 and 125, $\Delta\mathrm{RMS}_l$ of the three GOCE solutions and ITG-Grace2010s follow the same curve. This should be because of the error in EGM2008 as gravity models from GOCE and GRACE mission are individual uncorrelated (except for the GOCE direct solution which contains information from GRACE). It means that this comparison is not suitable for SH coefficients between degree 70 and 125 for using reference gravity model EGM2008. Thus another comparison results for the reference model of ITG-Grace2010s are shown in Figure 3.4.

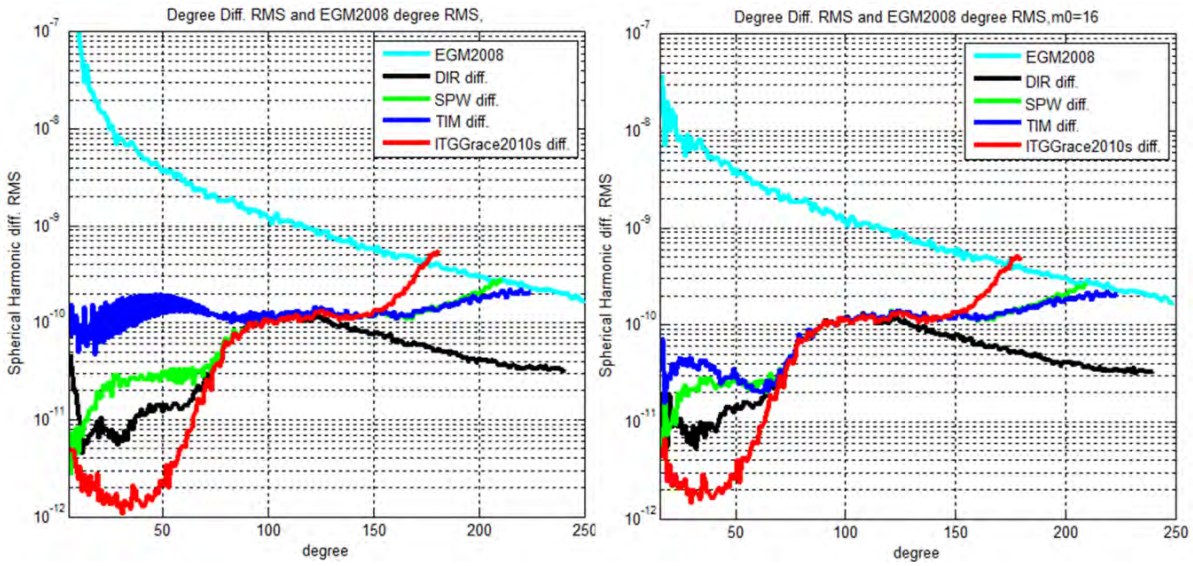

Figure 3.3: EGM2008 degree RMS and subtracted degree RMS of three GOCE solutions and ITG-Grace2010s w.r.t. EGM2008

In Figure 3.4, the left figure is for the full order and the right one with lower order terms ($m \leq 15$) eliminated. The time-wise solution oscillates significantly because of the polar gap. The oscillations because of the polar gap has been reduced when the near zonal coefficients are excluded when computing the $\Delta\mathrm{RMS}_l$. EGM2008 have larger differences comparing to GOCE solutions w.r.t. ITG-Grace2010s. All the GOCE solutions have similar behaviour over the degrees of 90. After degree 150 all the results of $\Delta\mathrm{RMS}_l$ grow rapidly as should be because of the error in the ITG-Grace2010s. EGM2008 has a small variation for degrees lower than 70 compared to GOCE solutions, this arises from the low accuracy of GOCE solutions for the low degrees of spherical harmonics.

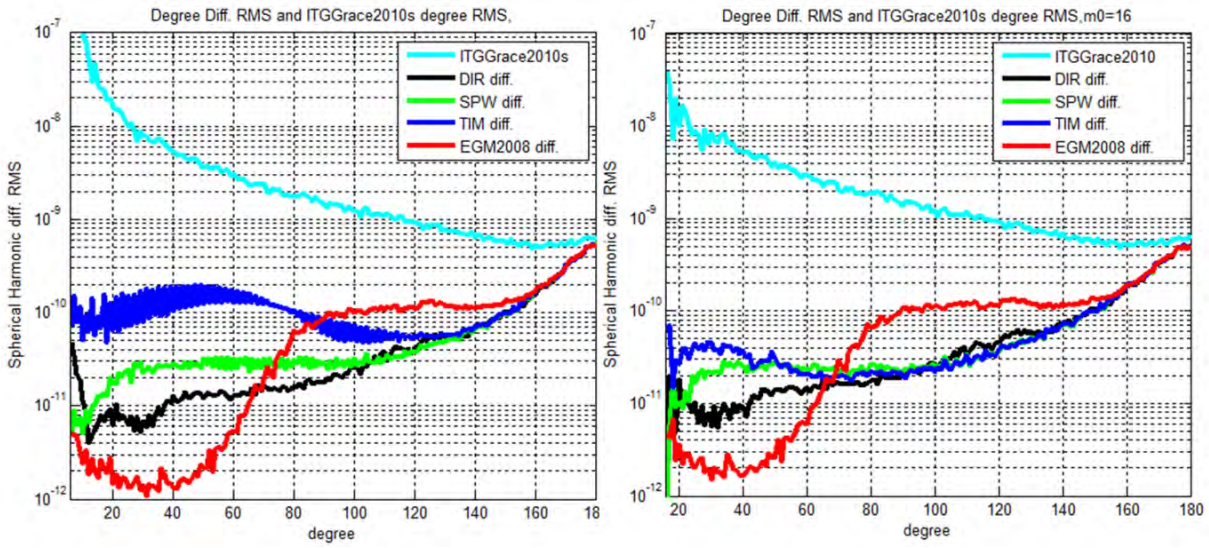

Figure 3.4: ITG-Grace2010s degree RMS and subtracted degree RMS of three GOCE solutions and EGM2008 w.r.t. ITG-Grace2010s

3.2 Global area comparison

The three GOCE solutions and ITG-Grace2010s are compared with EGM2008 in the spatial domain for understanding the spatial distribution of the residuals after the subtraction of EGM2008. The flow chart of the approach is shown in Figure 3.5. There is an alternative calculation procedure of subtracting the reference gravity model (EGM2008) in SC format, then synthesis to the $\Delta Geoid$.

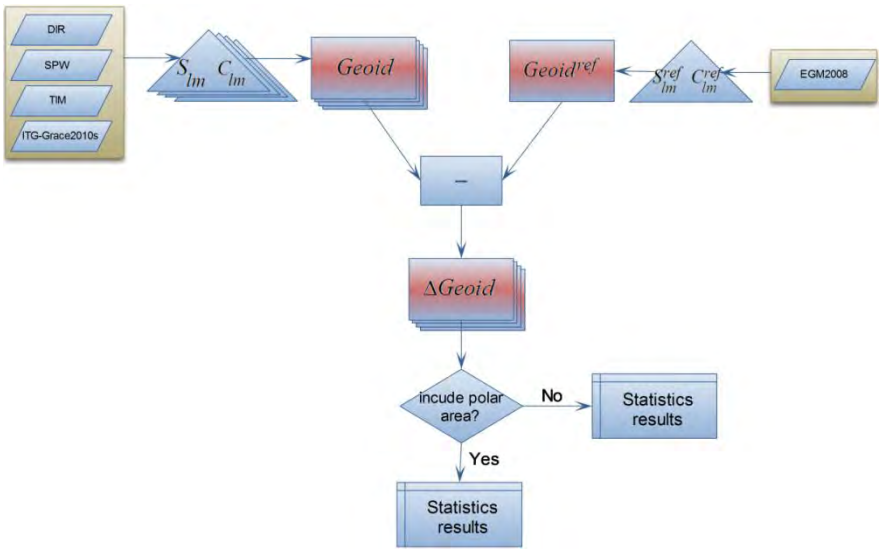

Figure 3.5: Working flow of direct spatial comparison for three GOCE solutions and ITG-Grace2010s with respect to EGM2008

The $\Delta Geoid$ with respect to EGM2008 for comparison up to degree 180 with polar areas (6.5 degrees of latitude) excluded is shown in Figure 3.6. EGM2008

shows a significant differences with respect to others gravity models in areas in Africa, South America and Himalayas where terrestrial gravity data is unavailable or not accurate (Pavlis, et al., 2008). Those significant differences were detected from GOCE solutions and GRACE gravity models which meant the differences stand for the improvements of the gravity fields with respect to EGM2008. Three GOCE solutions perform a better match to EGM2008 than ITG-Grace2010s globally up to degree 180.

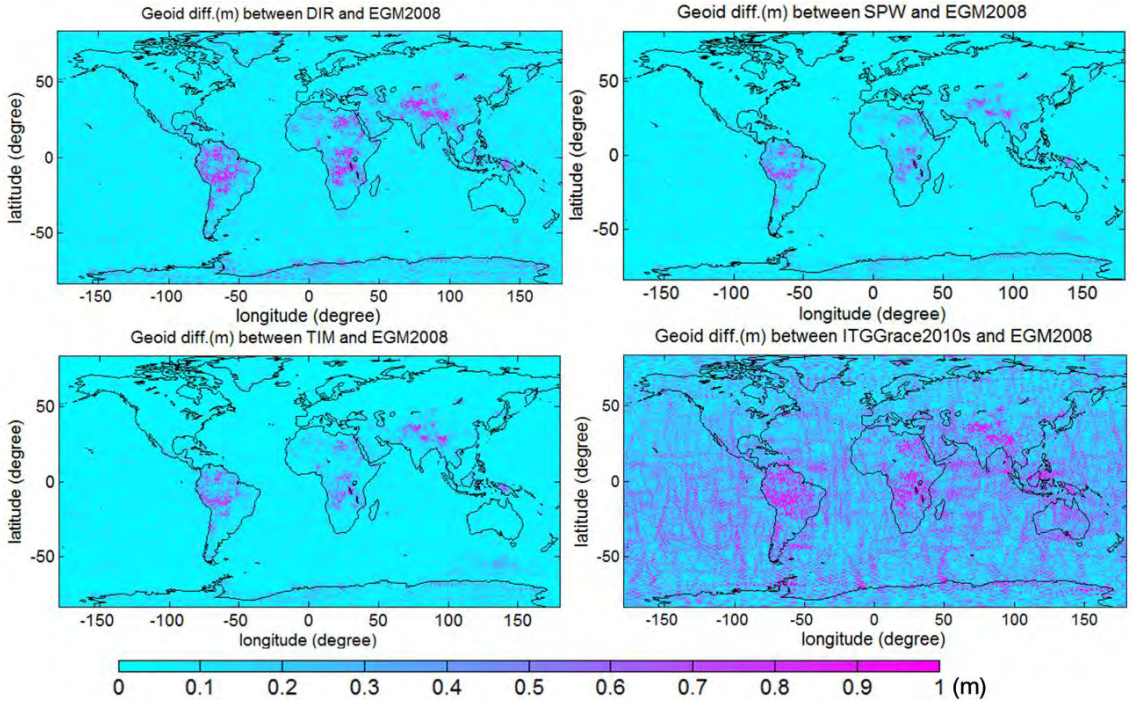

Figure 3.6: Geoid comparison for all gravity models synthesis up to degrees of 180 w.r.t. EGM2008

The pixel averaged RMS of $\Delta Geoid$ globally and with polar areas excluded ($\left|90^o - \theta\right| < 83.5^o$) up to degree 30, 60, 90, 120, 150 and 180 are shown in Table 3.1. After the elimination of polar areas, the difference between the time-wise solution and EGM2008 is reduced greatly. All the GOCE models are closer to EGM2008 than ITG-Grace2010s. Among those three GOCE solutions, the direct solution matches best to the EGM2008.

Geoids synthesized from each degree of SH coefficients from three GOCE solutions and ITG-Grace2010s are compared to the geoid from EGM2008 in the spatial domain. The results are similar to Figure 3.3 for the global $\Delta \mathrm{RMS}_l$. But the oscillation of the time-wise solution cannot be well reduced after excluding polar gaps of $6.5°$ degree latitude.

Table 3.1: Pixel averaged RMS of geoid comparison of three GOCE solutions and ITG-Grace2010s w.r.t. EGM2008

Geoid comparison w.r.t. EGM2008 globally (cm)						
Gravity models	**Up to degree**					
	30	**60**	**90**	**120**	**150**	**180**
DIR	0.4	0.6	2.0	5.1	7.0	8.2
SPW	0.5	2.2	4.3	7.2	10.1	13.0
TIM	7.4	28.8	44.4	45.8	46.4	47.3
ITG-Grace2010s	3.6	3.6	4.1	6.2	8.6	20.0
Geoid comparison w.r.t. EGM2008 without polar areas (cm)						
Gravity models	**Up to degree**					
	30	**60**	**90**	**120**	**150**	**180**
DIR	0.4	0.6	2.1	5.3	7.2	8.4
SPW	0.4	0.9	2.2	5.4	8.3	11.3
TIM	2.1	3.5	3.2	5.7	8.4	11.4
ITG-Grace2010s	3.4	3.4	3.9	6.2	8.7	20.4

The cumulative sum of the each degrees comparison is plotted In Figure 3.7. As ITG-Grace2010s has a big difference in the degree 2 SH coefficients, the lowest degrees are excluded in Figure 3.7. The geoids from all the gravity models are synthesized up to a certain degree and compared to EGM2008. From the result we can derive that the direct solution is stable after degree 125. From the results some significant improvements of the three GOCE gravity models can be found for high degrees (larger than 125 for the direct solution, larger than 160 for the space-wise and time-wise solutions). The space-wise solution has the best match to EGM2008 for degrees lower than 10 as in the space-wise solution EGM2008 used for degree variance modelling. Impact from the polar gap is reduced when the polar areas are excluded from the comparison between the right and left figures.

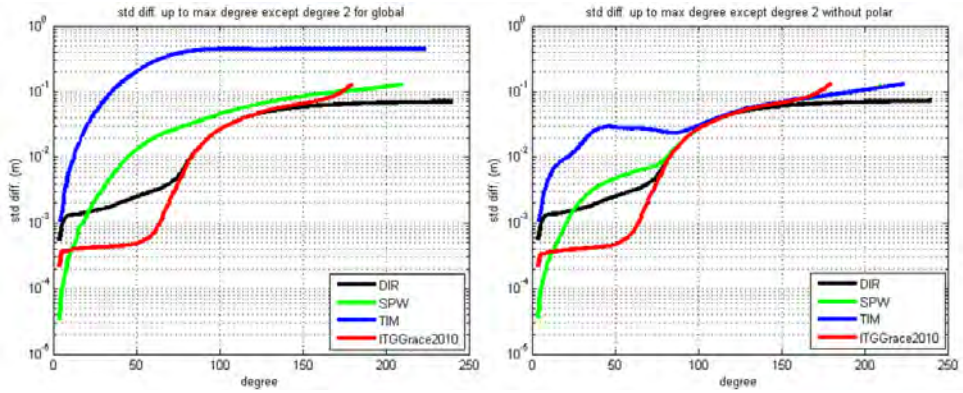

Figure 3.7: Standard deviations of the GOCE solutions and ITG-Grace2010s geoid differences w.r.t. EGM2008 synthesized up to a certain degree with degree 2 excluded

3.3 Local area comparison

The local area comparison will be limited to the area of the mid-Atlantic Ridge (Reykjanes Ridge) south-west of Iceland. The latitude of this area is in the range of $[55°, 65°]$ and the longitude is in the range of $[-45°, -15°]$. A topographic map derived from the Global Relief Data: TOPO2v2 (NOAA, 2006) from the National Geophysical Center of National Oceanic and Atmospheric Administration (NOAA) is plotted in the left of Figure 3.8. A geopotential map is synthesized from the GOCE direct solution up to degrees of 240 (full degrees). From the topographic map, Reykjanes Ridge is a clear and sharp signal under the Atlantic Ocean. The corresponding geopotential map shows a clear signal which is similar to the ridge structure which is the result from the Reykjanes Ridge. The GOCE gravity models have a spatial resolution of 100 km, which means most of the Reykjanes Ridge is signal in the gravity field model. More information about mid-oceanic ridges can be found in (Turcotte & Schubert, 2002).

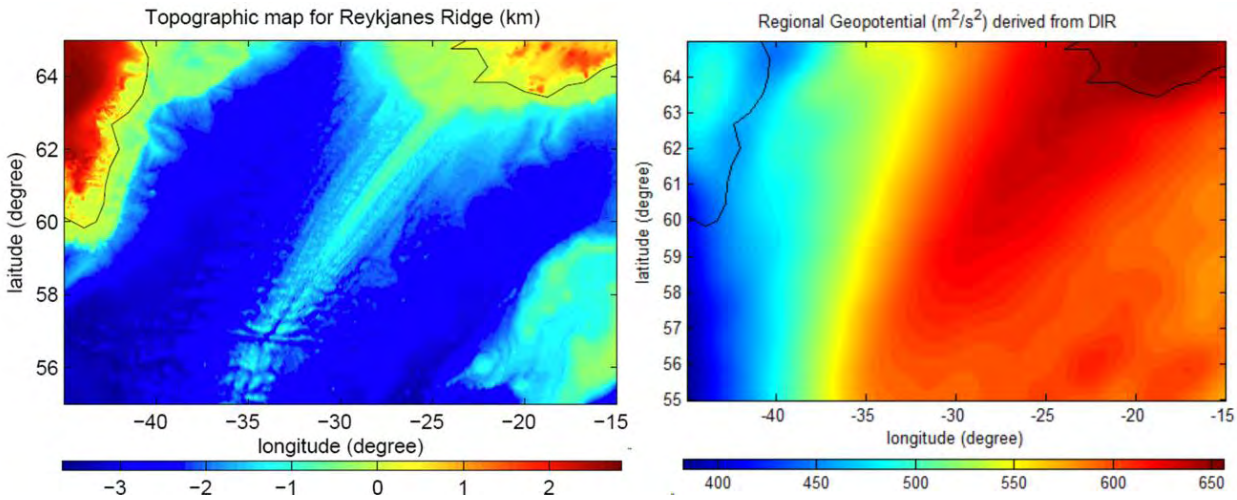

Figure 3.8: Topographic and geoid map in the area of Reykjanes Ridge

3.3.1 Geophysical model comparison

A simplified parametric geophysical model is used to see if the gravity signal can be approximated with a geophysical model. This model is derived from the treatment of mid-ocean ridges in a geodynamic textbook (Turcotte & Schubert, 2002). The temperature profile of the lithosphere with horizontal heat conduction neglected from Eq. 4-124 in (Turcotte & Schubert, 2002) can be presented as

$$\frac{T_1 - T}{T_1 - T_0} = \operatorname{erfc}\left(\frac{y}{2\sqrt{\kappa x / u}} \right) , \tag{3.3}$$

where T_0 is the surface temperature, T_1 is the mantle temperature, y is the depth of the lithosphere, κ is the thermal diffusivity, x is the horizontal distance and u is the spreading rate.

The relation between the ocean depth and temperature using the principle of isostasy from Eq. 4-209 in (Turcotte & Schubert, 2002) is

$$w = \frac{2\rho_m \alpha_v (T_1 - T_0)}{\rho_m - \rho_w} \sqrt{\frac{\kappa t}{\pi}} , \tag{3.4}$$

with w the ocean depth, ρ_m the density of the mantle, α_v the volumetric coefficient of thermal expansion and t the age of the lithosphere.

The gravitational potential perturbation, ΔV , can be derived from

$$\Delta V = 2\pi G \left\{ \int_{-w}^{0} y(\rho_w - \rho_m) dy + \int_{0}^{\infty} y(\rho - \rho_m) dy \right\} , \tag{3.5}$$

with ΔV the gravitational potential perturbation, G the gravitational constant.

Inserting Eqs. (3.3) and (3.4) into Eq. (3.5) yields the gravitational potential perturbation as a linear function of distance from the ridge shown in Figure 3.9,

$$\Delta V = -\frac{2\rho_m (T_1 - T_0)}{\pi(\rho_m - \rho_w)} \frac{g}{u} s \ , \tag{3.6}$$

with spreading rate $u = 1\,\mathrm{cm/year}$ (Talwani, Windisch, & Langseth, 1971), mantle density $\rho_m = 3300\,\mathrm{kg/m^3}$,temperature difference $T_1 - T_0 = 1200\,\mathrm{K}$, thermal expansion coefficient is $\alpha = 1\times10^{-5}\,\mathrm{K^{-1}}$, thermal diffusivity is $\kappa = 1\times10^{-6}\,\mathrm{mm^{-2}/s}$.

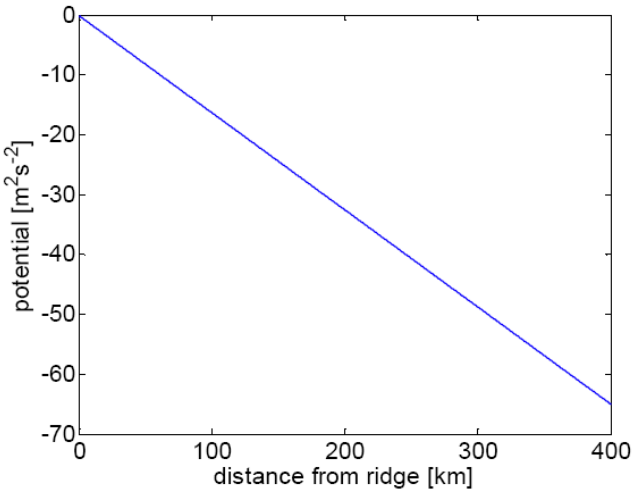

Figure 3.9: Potential perturbation relative to the distance from Reykjanes ridge

From Figure 3.9, the center of ridge has the largest gravitational potential which also provides a method of determining the center of ridge. Different gravity models have different gravitational potential distributions and yield different ridge centers. The results of the different center lines of Reykjanes ridge are shown in Figure 3.10. The ridge center lines derived from gravity models do not fully follow the ridge from the topography data, and the ridge center lines will be derived from each gravity model. The ridge center line from the ITG-Grace2010s has a different behaviour comparing to the center lines from other gravity models. It is clear that the GOCE solutions have less noise than GRACE model (ITG-Grace2010s); the three ridge center lines from the GOCE gravity models are almost straight and close to EGM2008.

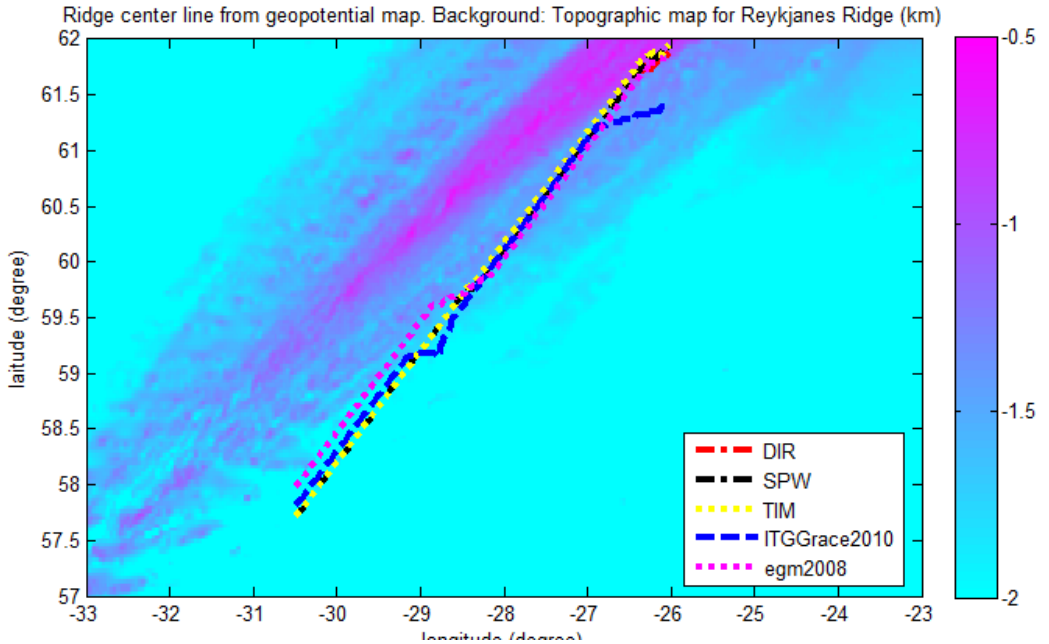

Figure 3.10: Center of Reykjanes ridge derived from gravity models: 3 GOCE solutions, ITG-Grace2010s and EGM2008 up to degree 180, background: ocean depth from TOPO2v2

For comparison with respect to geophysical model shown in Figure 3.9, five tracks are selected and plotted in Figure 3.11.

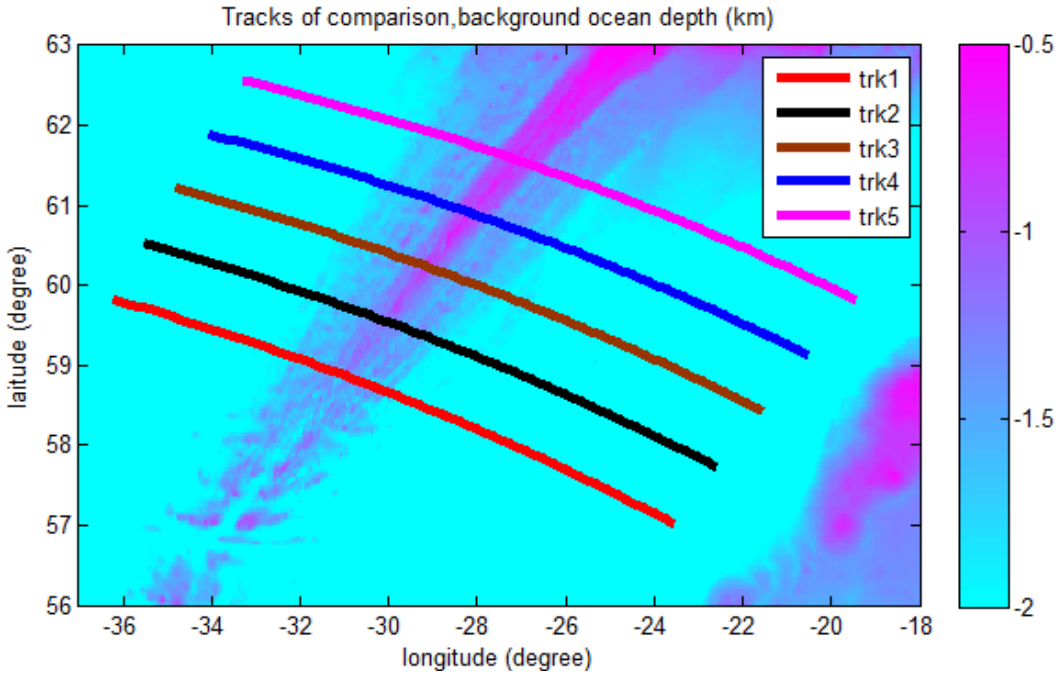

Figure 3.11: Selected tracks for comparing gravitational potential w.r.t. geophysical model, background: ocean depth from TOPO2v2

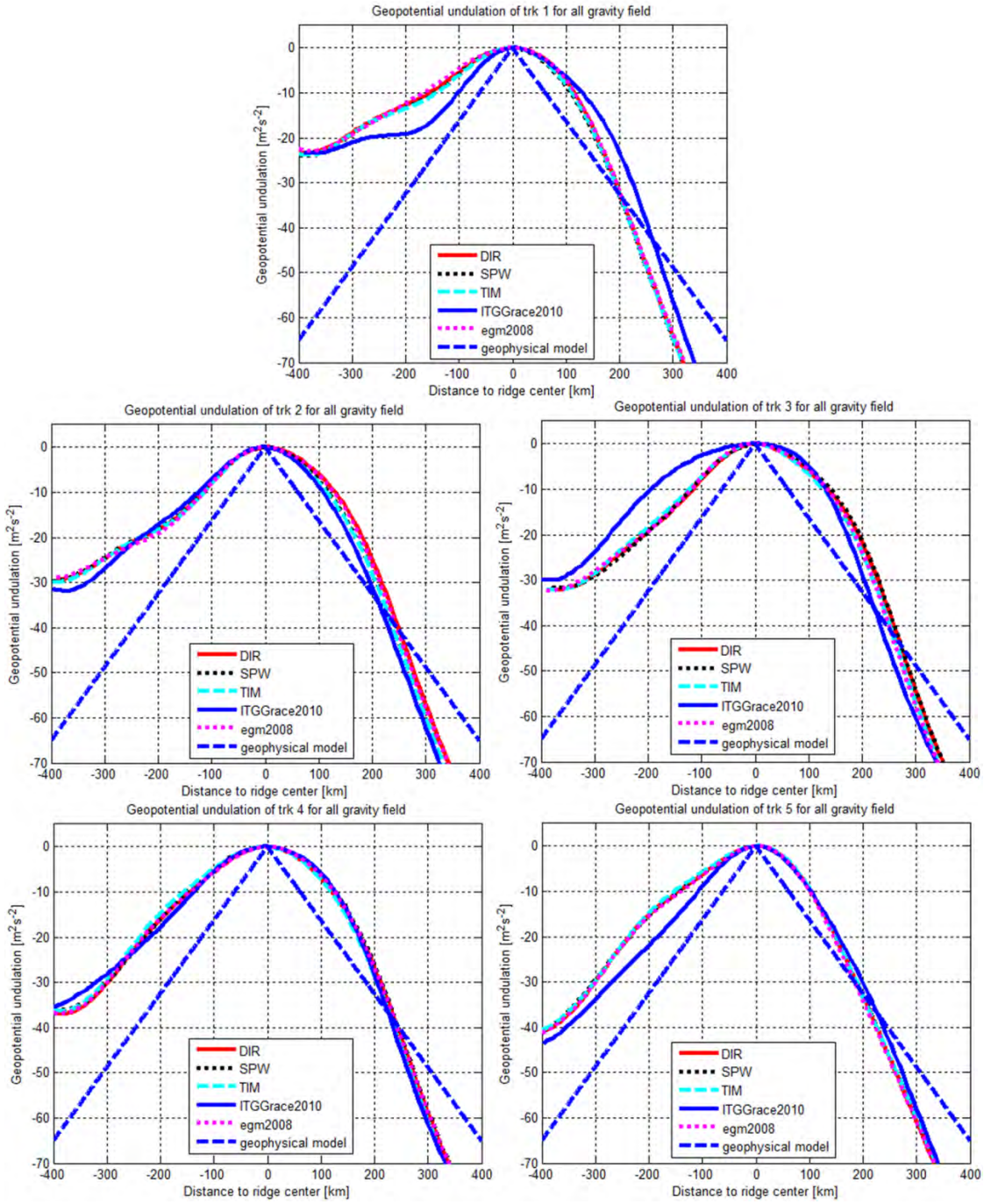

Figure 3.12: Geopotential undulation of five tracks described in Figure 3.11 for each gravity field model

From Figure 3.12, the geophysical model fits better northwest of the ridge compared to southeast. From track 1 to track 5, the geopotential undulation derived from all gravity models gets closer to geopotential model, thus geophysical model fits better when the latitude is higher for the northwest direction. Five geopotential undulation tracks from three GOCE gravity field solutions and EGM2008 have similar behaviour. The tracks from ITG-Grace2010s are apart from the tracks from the other four models. The difference between the tracks derived from geophysical model and from gravity field models

might come from the simple constant density assumption. In reality mantle and lithosphere densities vary over locations. The difference between the geopotential undulations from geophysical model and the gravity models are mainly low wavelength signal. Subtraction of lowest degree might lead a better match.

3.3.2 Gravity models comparison

Geoids synthesized from the gravity models are used for the comparison in the local area. The approach of the comparison is similar to the procedure shown in Figure 3.5, but within a local area. The results of geoid differences with respect to EGM2008 are shown in Figure 3.13. The geoid difference of ITG-Grace2010s with respect to EGM2008 is larger than the geoid difference of the GOCE solutions. From the results no linear pattern can be found that resembles the Reykjanes Ridge, thus it seems that no remaining geophysical signal can be found from the GOCE solutions. The geoid differences from 3 GOCE solutions contain several linear patterns along the Greenland coastline while the result of the ITG-Grace2010s shows artificial patterns that do not resemble any geophysical signal and are partly due to the omission error. This artificial effect can also be seen from other comparisons between three GOCE solutions and EGM2008, but smaller. In order to avoid this effect, a Gaussian filter method (Wahr, Molenaar, & Bryan, 1998) is used in the spectral domain for the SH coefficients. The results after Gaussian filtering are shown from Figure 3.14 to Figure 3.17.

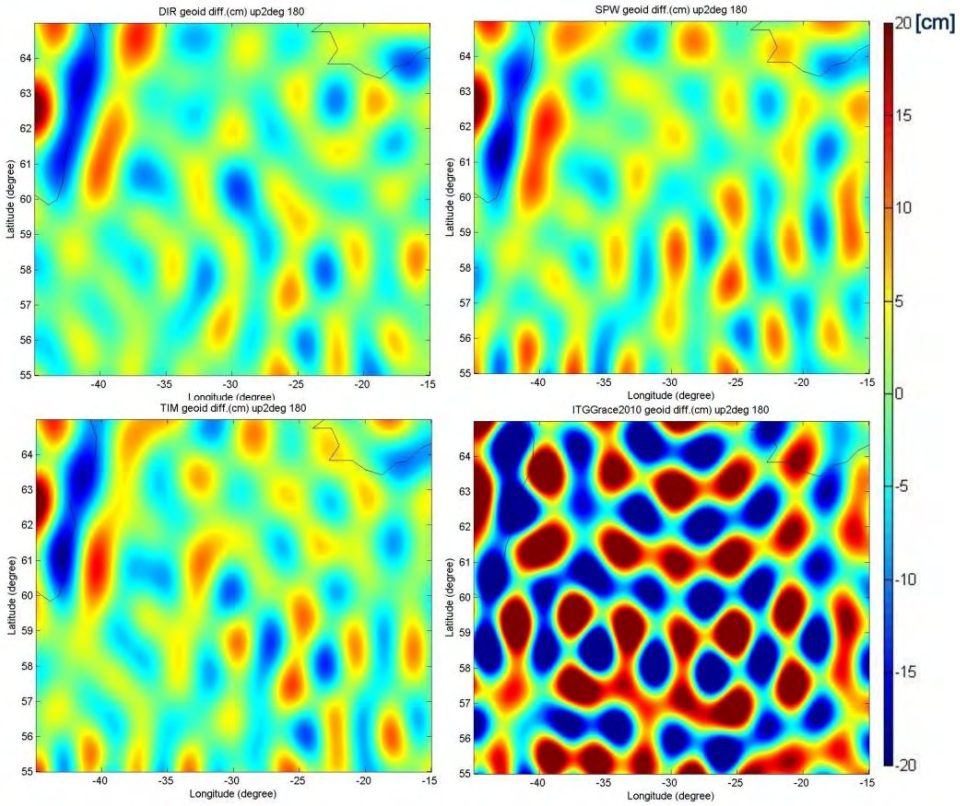

Figure 3.13: Local geoid difference of GOCE solutions and ITG-Grace2010s up to degree 180 w.r.t. EGM2008

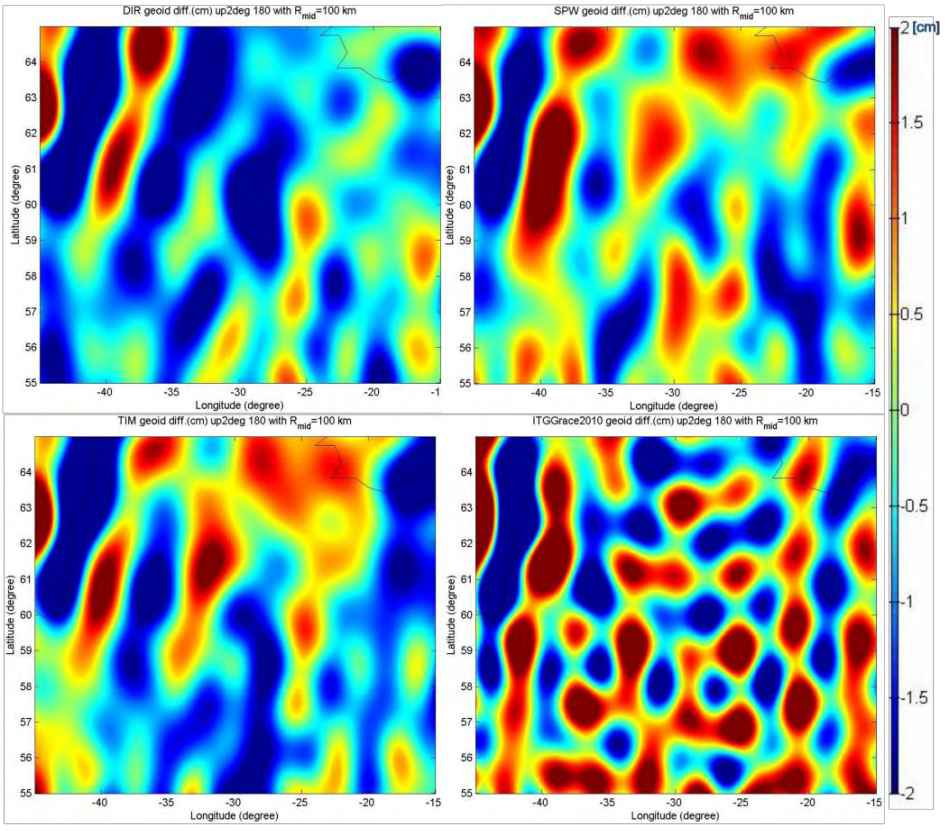

Figure 3.14: Local geoid comparison w.r.t. EGM2008 synthesized up to degree 180 after 100 km Gaussian smooth filter

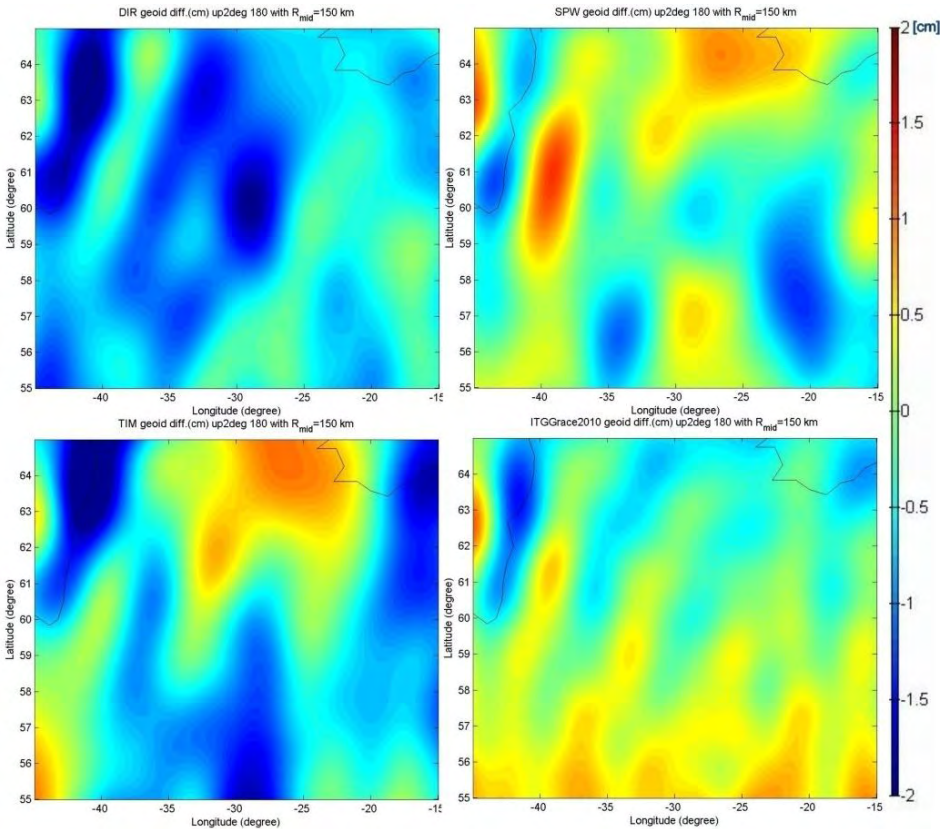

Figure 3.15: Local geoid comparison w.r.t. EGM2008 synthesized up to degree 180 after 150 km Gaussian smooth filter

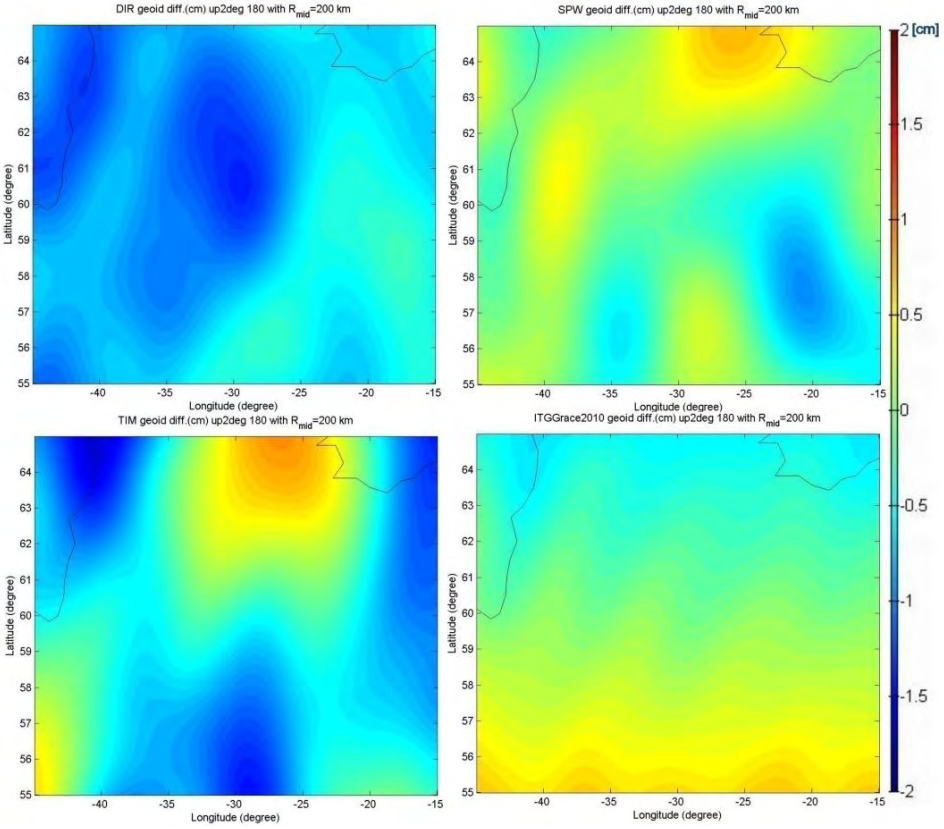

Figure 3.16: Local geoid comparison w.r.t. EGM2008 synthesized up to degree 180 after 200 km Gaussian smooth filter

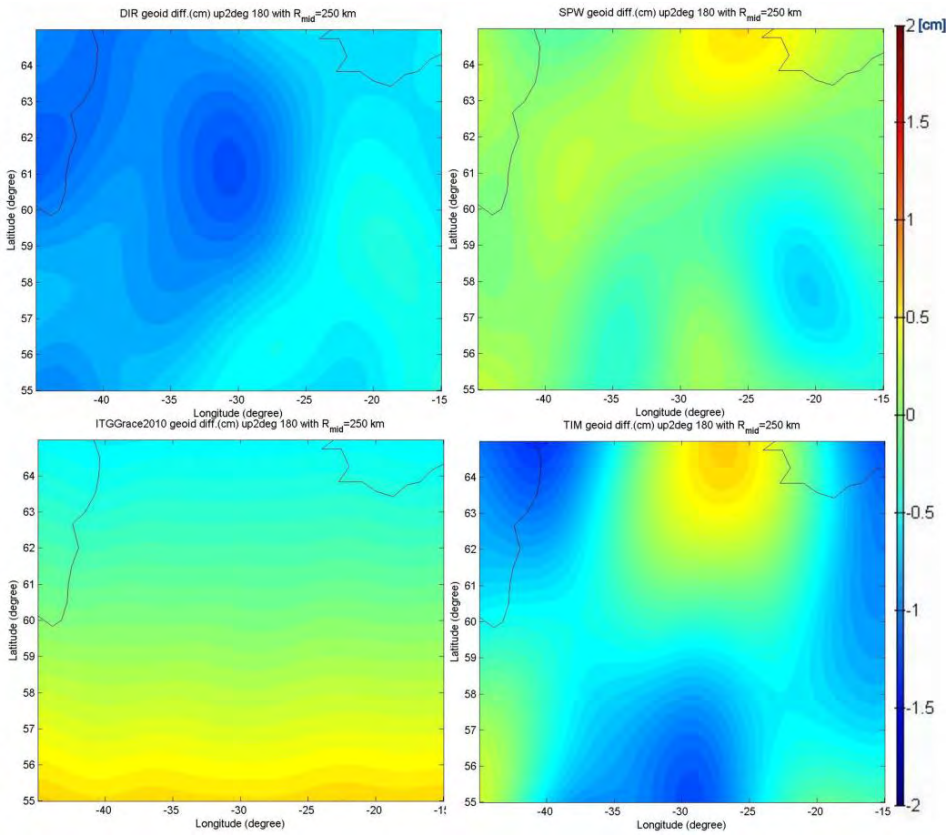

Figure 3.17: Local geoid comparison w.r.t. EGM2008 synthesized up to degree 180 after 250 km Gaussian smooth filter

From the results shown from Figure 3.14 to Figure 3.17, differences with respect to EGM2008 follow the Greenland coastline in shape and with much larger amplitude than in the rest of the area. EGM2008 is created from several data sources: satellite altimetry on the coast with terrestrial data on land. Satellite altimetry data have poorer quality near the coast than in the open ocean. Thus the linear pattern is possible the result from artificial piecing together different datasets in EGM2008. Differences from three GOCE solutions are smaller than ITG-Grace2010s model with respect to EGM2008. This area consists mainly of ocean and EGM2008 contains satellite altimetry observations there which have a good quality. It means that the three GOCE solutions are better than ITG-Grace2010s for this area up to SH degree and order 180.

3.3.3 Ship track comparison

For a more detailed comparison, ship track measurements are used for assessment in the local area. The ship-borne data is from the National Geophysical Data Center, NOAA. The following items are used in this comparison: time t, co-latitude θ, longitude λ, gravity anomaly $\overline{g}$ and the

standard deviation of the gravity observation $\sigma_{\bar{g}}$. Gravity models are synthesized at the location of the ship tracks. The work flow is shown in Figure 3.18.

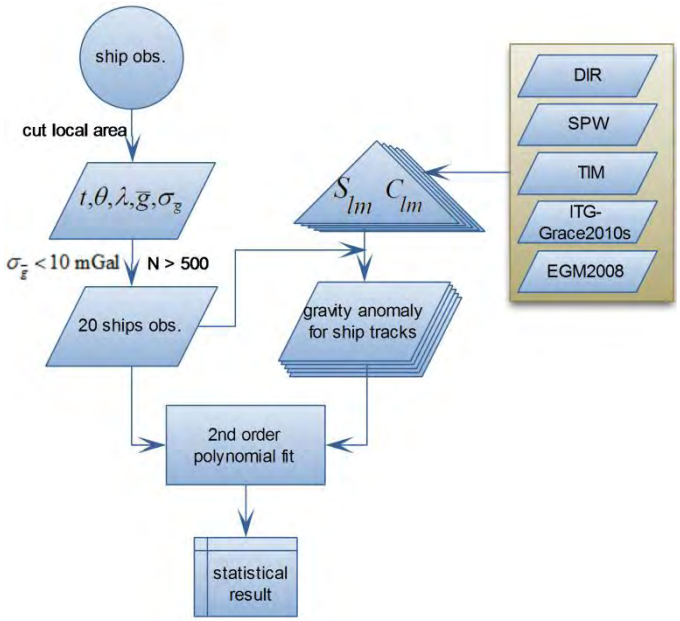

Figure 3.18: Working flow of ship tracks comparison

The 20 ship tracks are selected after cutting the local area and with the condition of the number of observation points, $N > 500$ and a standard deviation of the gravity anomaly, $\sigma_{\bar{g}} < 10\,\mathrm{mGal}$. All the tracks are plotted in Figure 3.19 with the background showing the ocean depth.

A 2nd order polynomial fit is used for comparing the gravity anomaly from the geopotential models to the ship borne observations of the 20 ship tracks. The differences between gravity anomaly from the ship borne observation and from gravity models are modelled are presented as following,

$$g_{ref}^{t} - g_{ship}^{t} = b_0 + b_1 t + b_2 t^2 + \varepsilon \quad , \tag{3.7}$$

where t is the time epoch of the observation, g_{ship}^{t} is the gravity anomaly from the observation of ship at time t, g_{ref}^{t} is the gravity anomaly derived from the gravity models at time t, (b_0, b_1, b_2) are the bias, drift and quadratic term with time, ε is the residuals after polynomial fit. ε will be used for estimating the statistical result shown in Figure 3.18.

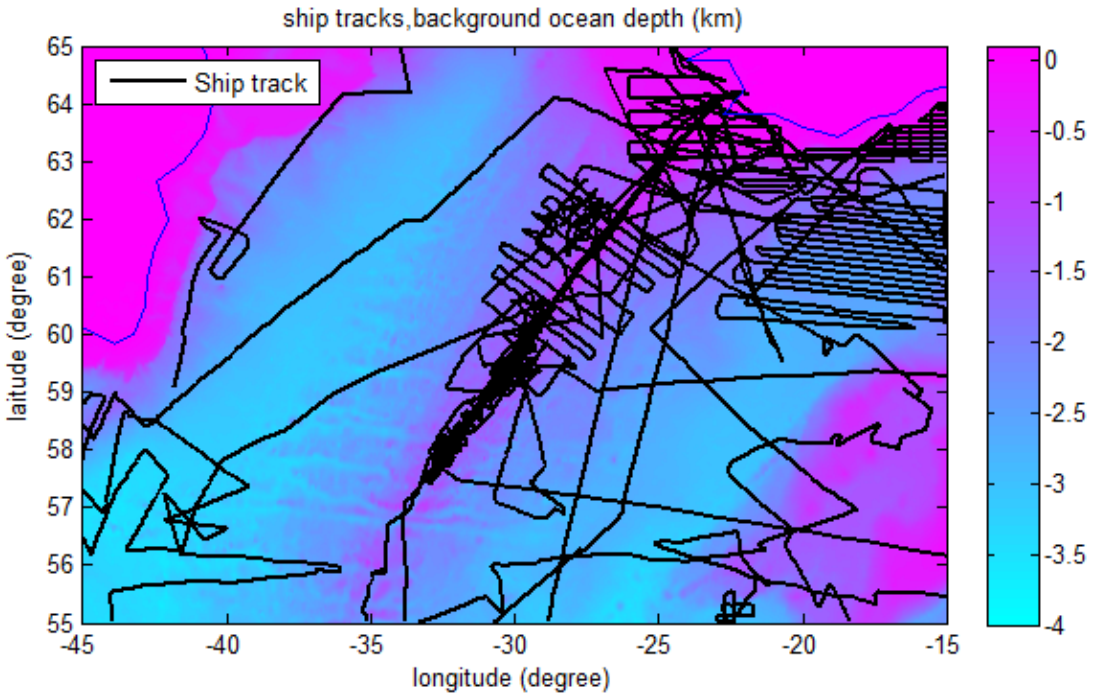

Figure 3.19: 20 ship tracks with background of ocean depth (km) from TOPO2v2

For the full time series the ship observation errors will be a vector $\boldsymbol{\varepsilon}$, the differences of g^t_{ship} and g^t_{ref} are considered as observations vector $\mathbf{y}$, then the observation model can be presented as following,

$$\mathbf{y} = \mathbf{A}\begin{bmatrix} b_0 \\ b_1 \\ b_2 \end{bmatrix} + \boldsymbol{\varepsilon}, \quad \mathbf{A} = \begin{bmatrix} 1 & t_1 & t_1^2 \\ 1 & t_2 & t_2^2 \\ \vdots & \vdots & \vdots \end{bmatrix} \quad \mathbf{y} = \begin{bmatrix} g^{t_1}_{ref} - g^{t_1}_{ship} \\ g^{t_2}_{ref} - g^{t_2}_{ship} \\ \vdots \end{bmatrix}. \tag{3.8}$$

For estimating the error, Least Squares adjustment is used,

$$\boldsymbol{\varepsilon} = \mathbf{y} - \mathbf{A}(\mathbf{A}^T\mathbf{A})^{-1}\mathbf{A}^T\mathbf{y} \quad . \tag{3.9}$$

For each track, it is possible to compute five error matrices, $\boldsymbol{\varepsilon}$, for the five gravity models. Then the standard deviation of the error matrices, σ_ε, can be computed and it shown in Table 3.2. Two outliers are detected: SHACK877 and STA179B show unreasonable differences from all gravity models. The results show a good agreement with gravity models as most of the σ_ε are around the 10 mGal level. ITG-Grace2010s shows a better match with the ship tracks and no improvement of GOCE dataset can be detected from this comparison which could be because the lower degrees of SH coefficients have a larger amplitude and the long ship track distance fall in the range of the low degrees. Moreover, the ship track measurements have too much error to evaluate GOCE data, as the standard

deviation of difference between EGM2008 and ITG-Grace2010 is around 2mGal which is much larger than the standard deviation of the ship measurements.

Table 3.2: Standard deviations of ε (mGal) after 2nd order polynomial fit, bold numbers highlight the lowest standard deviations, TOTAL result excludes SHACK877 and STA179B. The last column shows the difference between EGM2008 and ITG-Grace2010s

Ship tracks ID	DIR	SPW	TIM	EGM2008	ITG-Grace2010s	Ref. data diff.
CD5290	21.4	**21.2**	21.3	21.4	22.5	1.6
CD8093	13.2	13.0	13.2	13.4	**12.1**	0.7
DI84L1-2	9.7	9.6	9.6	9.6	**9.5**	1.2
DUT02-71	19.5	19.3	19.4	**19.0**	**19.0**	1.2
EW9004	11.9	11.9	12.0	11.8	**11.3**	0.9
EW9005	7.7	7.6	7.5	8.1	**6.5**	1.9
EW9006	15.0	14.2	14.4	14.1	**13.0**	1.0
EW9008	14.7	**14.6**	14.7	**14.6**	**14.6**	1.4
KEA01-72	16.2	15.9	16.0	15.5	**14.9**	2.5
KEA10-71	10.9	11.0	11.1	11.1	**10.3**	0.9
KEA11-71	7.8	7.6	7.8	7.7	**7.3**	1.9
KT1	**7.7**	7.8	7.9	7.9	**7.7**	0.6
SHACK877	104.3	104.0	104.2	104.2	103.7	0.7
STA179B	155.8	155.8	156.0	155.7	157.1	2.4
V2303	11.4	11.3	11.3	**11.2**	11.7	1.1
V2702	10.8	10.8	10.8	**10.7**	12.2	1.5
V2706	13.1	**13.0**	**13.0**	13.2	13.1	1.6
V2909	12.1	12.2	12.1	**11.9**	12.2	0.6
V2911	**9.2**	**9.2**	**9.2**	9.3	9.8	1.0
V3008	12.0	**11.9**	12.0	**11.9**	13.1	1.4
TOTAL	13.58	13.41	13.52	13.56	**13.07**	1.2

Chapter 4. GOCE gravity gradient assessment

In this chapter the gravity gradient from GOCE level 2 products (see section 1.2) will be the assessed. The reference gravity model for assessment will be EGM2008 up to degree 300 which corresponds to 67 km spatial resolution. The GOCE gradiometer measurement bandwidth is 5–100 mHz. As the speed of GOCE mission is about 7.6 km/s the bandwidth of 5–100 mHz stands for 76–1500 km in orbit.

Visser (2011) analyzed GOCE gravity gradient data in Nov. 2009 and Dec. 2009 with prior gravity models (EIGEN5C and ITG-Grace2010s) and found that very detailed gravity field signatures can be observed from these two months of observation. The RMS of differences between the GOCE observed gradients and prior gravity models in the measurement bandwidth of 10-100 mHz are within the range of 3-7 mE. Müller, et al. (2010) used methods of cross-over analysis and upward continuation of terrestrial gravity data monitoring the quality of GOCE gradients, found the radial tensor component is well below the required accuracy level.

The selection of the band-pass filter will be discussed in section 4.1. A comparison between the Butterworth and Chebyshev type I and II low-pass filter will be shown in this section. Butterworth band-pass filter of different degrees and the its application to GOCE gravity gradient will also be introduced. Section 4.2 will compare the gravity gradient for the repeat tracks.

4.1 Band-pass filter selection

In order to limit the gravity gradients to the bandwidth of gradiometer, the gravity gradients from the gradiometer should be filtered before use. Specific filters have to be applied according to the type of the data source and application. Different filters will also have different influences on filtered results. It is also required to remove the out-band signals with minimal side effects on the pass-band signal. Directly filtering the gravity gradients along the orbit considering the gravity gradients as a time series signal is so-called along-track filtering.

There are several band-pass filters that can be applied to a discrete dataset, such as the Bessel filter, Elliptic filter, Butterworth filter, Chebyshev filter and so on. A Bessel filter is often used in audio crossover systems like speakers as it has a constant group delay across the entire pass band, thus preserving the wave shape of filtered signals in the pass band. An Elliptic filter, also known as Cauer filter, is a signal processing filter with equalized ripple behaviour in both pass and stop band. Butterworth filter and Chebyshev filter will be discuss in more details following. Because of the lack of time, other filters will not be discussed in detail.

The Butterworth filter is a common filter first described by S. Butterworth (1930). The magnitude response of the Butterworth filter is flat in the pass band without ripples and rolls off towards zero in the stop band. The Butterworth low-pass filter‟s magnitude response is expressed by

$$\left|H(\omega)\right|^2 = \frac{1}{1+(\omega/\omega_c)^{2N}} \quad , \tag{4.1}$$

with $H(\omega)$ the magnitude response for frequency ω, ω_c the cut-off frequency (-3 dB) and *N* the filter degree which specified the roll-off „speed‟. The higher the *N*, the sharper the roll-off „speed‟ is (see Figure 4.2).

Chebyshev type I & II low-pass filters are other common filters in signal processing and widely used in many research fields. Chebyshev type I & II filters are named in honour of P. Chebyshev because the filters‟ mathematical characteristics are derived from Chebyshev polynomials. They have a steeper roll-off and more pass-band ripple (type I) or stop-band ripple (type II) than Butterworth filters. The Chebyshev type I filter has an amplitude response function,

$$\left|H(\omega)\right|^2 = \frac{1}{1+\varepsilon^2 T_N(\omega/\omega_c)} \quad , \tag{4.2}$$

Where ε is the ripple factor and $T_N()$ is a Chebyshev polynomial of the order N.

The amplitude response of the Chebyshev type II filter is

$$\left|H(\omega)\right|^2 = \frac{1}{1+\left(\varepsilon^2 T_N(\omega/\omega_c)\right)^{-1}} \quad . \tag{4.3}$$

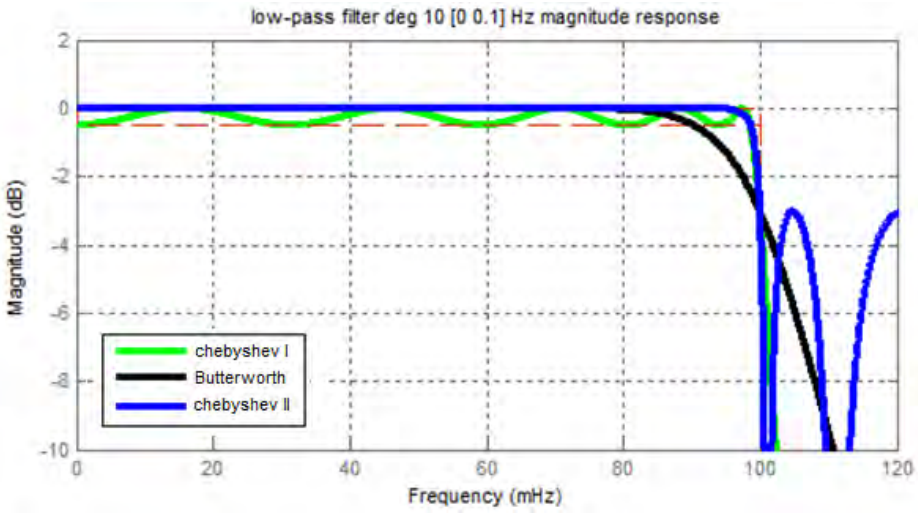

Figure 4.1: Low-pass filters with degree 10 and cut-off frequency of 100 mHz

In Figure 4.1, three low-pass filters have been plotted with the degree 10 and a cut-off frequency $f_c = f_{-3\mathrm{dB}} = 100\,\mathrm{mHz}$ (The maximum frequency of the measurement bandwidth). For the Chebyshev type I filter, the amplitude of the ripples in the pass-band was select to be ε=0.5 dB. For the Chebyshev type II filter, the stop frequency was selected to be $f_{stop} = 200\,\mathrm{mHz}$. It is clear that the Chebyshev type I filter has ripples in the pass band and it means that the ripples will affect the original signal. This does not meet the requirement of removing the out band signals and keeping the original signals. The Chebyshev type II filter has a shape decrease at the cut-off frequency but the ripples in the stop band yield residual from the out band in the filtered result. Finally, the Butterworth filter was selected to be applied to the gravity gradients, although the Butterworth filter does not have a steep roll-off wave, which results in the filtered dataset containing some out band signal. This can be improved by using a proper degree.

The band-pass filter can be obtained from the low-pass filter via the bandform transformation (Champagne, Labeau, & Peter, 2004; Oppenheim & Shaffer, 1999). In this thesis, we used the MATLAB signal processing toolbox to generate the filter and the following analysis.

From Eq. (4.2), Butterworth filter"s degree N needs to be specified. N affects the „speed" of the roll-off. A set of Butterworth band-pass filters of degrees of 4, 6, 10, 20 and 30 is plotted in Figure 4.2. The higher degree of the filter, the steeper the decline of the amplitude response around the cut-off frequency is. It means that for higher filter degree the signal above the cut-off frequency will affect less the signal within the measurement bandwidth.

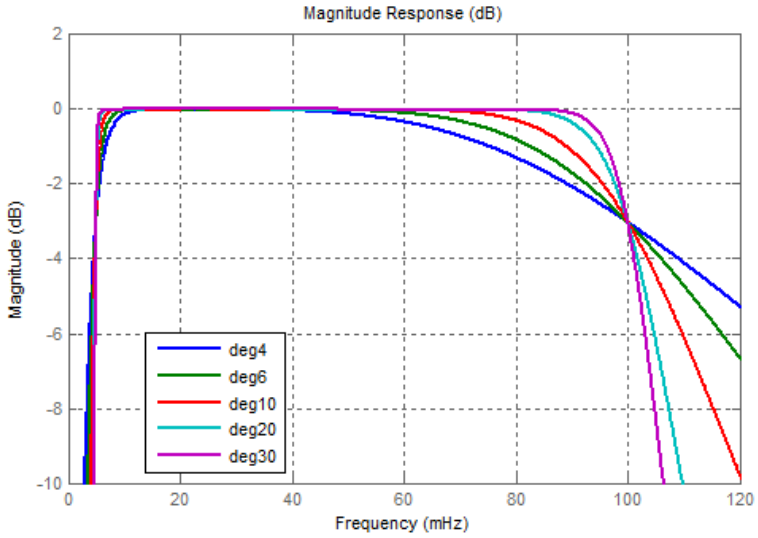

Figure 4.2: Butterworth band-pass filters" magnitude response with cut-off frequencies [5 100] mHz for degrees of 4, 6, 10, 20 and 30

In order to find a proper degree for the band-pass filters, an analysis in frequency domain will be necessary. The sampling frequency of the gravity gradients in Level 2 products is 1 Hz and the gradients are discrete observations. We use Fast Fourier transform (FFT) to convert gradients from the time domain to the frequency domain. The procedure of the comparison in the frequency domain is shown in Figure 4.3 and corresponding results are in Figure 4.4.

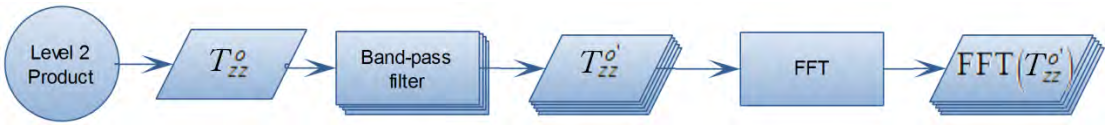

Figure 4.3: Work flow of comparing the gravity gradients after band-pass filtering in the spectral domain

In Figure 4.4, the gravity gradients without filtering have a strong signal out of the measurement bandwidth. For low frequency ($\omega < 5$ mHz), the gravity gradients have the maximum amplitude up to about 5000 E. The amplitude Ap of the high frequency is not zero because of the noise, $Ap \approx 0.5$ mE when $\omega = 100$ mHz and $Ap \approx 0.25$ mE when $\omega = 200$ mHz. After the degree 4 and 6 Butterworth band-pass filter, the Ap in the low frequency is reduced but still peaks can be found in low frequency range of the filtered result in spectral domain. After the degree 10 filter, the peaks below 2.5 mHz are removed and the shape of the filtered result $\mathrm{FFT}(T_{zz})$ for $5\ \mathrm{mHz} < \omega < 100\ \mathrm{mHz}$ remains comparable to low degree (N=4,6) Butterworth band-pass filters which means that the degree 10 filter has a small effect within the measurement bandwidth. After the degree 20 filter, Ap has a small shift for $5\ \mathrm{mHz} < \omega < 7\ \mathrm{mHz}$. The $\mathrm{FFT}(T_{zz})$ after the degree 30 filter has a wrong amplitude in the low frequency part ($\omega < 7$ mHz).

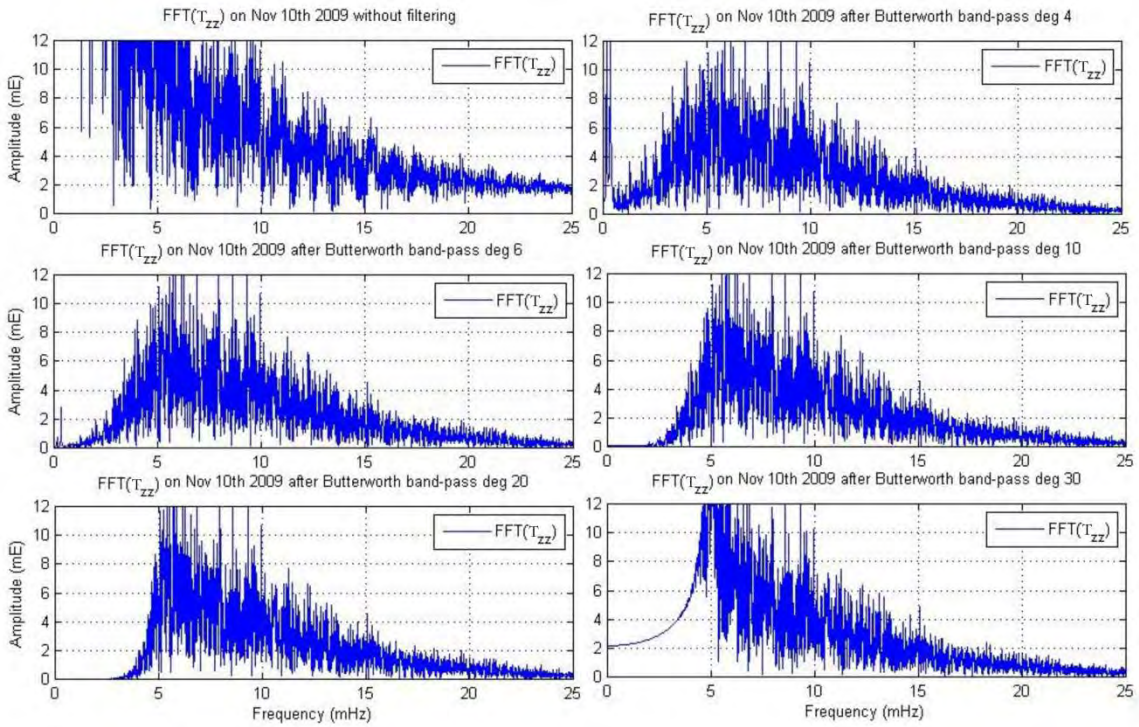

Figure 4.4: Nov 10th 2009 gravity gradients in spectral domain after the Butterworth band-pass filters in degrees of 4, 6, 10 and 20.

4.2 Repeat track comparison

GOCE orbits in a two-month repeat orbit and during repeat period the global and regional gravity field does not change much. It is possible to compare the SGG from sets of repeated orbit tracks to study the noise in the GOCE signal. The repeat tracks comparison will be limited to the local area of the Reykjanes Ridge rather than the global area. In the area of the Reykjanes Ridge, 16 sets of GOCE orbit tracks are selected for the comparison for the two time period, Nov. 1, 2009 to Dec. 2, 2009 and Jan. 13 to Feb. 2, 2010. 16 tracks within the period of Jan. 13 to Feb. 2 2010 are plotted in Figure 4.5 with the background geoid undulation map derived from the GOCE direct solution.

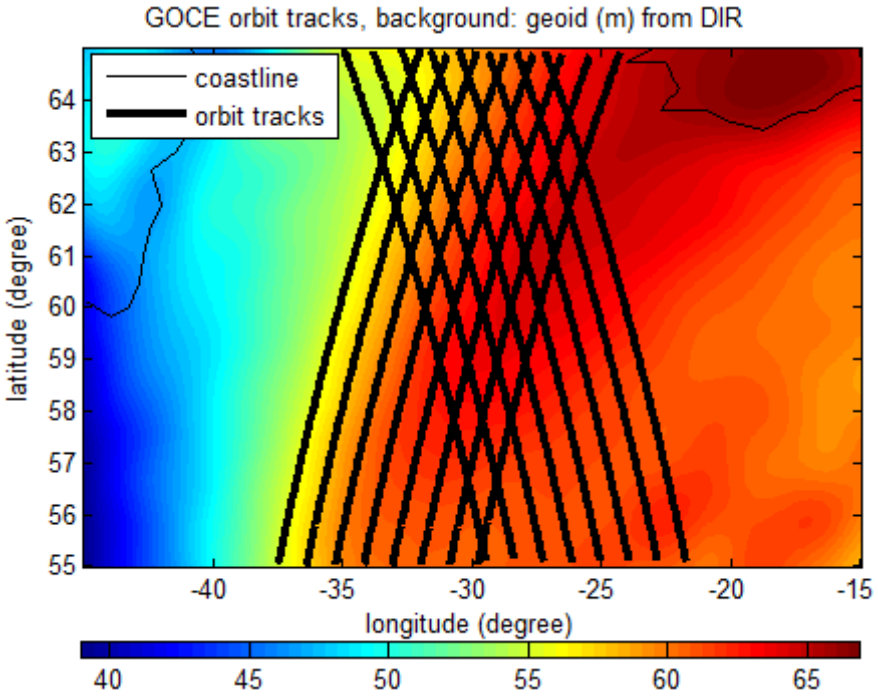

Figure 4.5: GOCE orbit tracks with background of geoid derived from DIR

The gravity gradients between one set of repeat tracks in GRF, $x^q = (x, y, z)$, can be modelled by

$$\mathbf{T}_{x^q}^{t_2}(P) = \mathbf{T}_{x^q}^{t_1}(P') + \delta\mathbf{T}_{x^q}(\delta P) + \delta\mathbf{T}_{x^q}^{t_{12}}(P) + \varepsilon \ , \tag{4.4}$$

with P and P' the observed positions in GRF for t_2 and t_1, respectively; t_1 and t_2 the times for first pass and second pass, respectively; $\delta\mathbf{T}_{x^q}^{t_2}(P)$ the gravity gradient matrix in GRF at location P at time t_2 which is the second pass; $\delta\mathbf{T}_{x^q}^{t_1}(P')$ the gravity gradient tensor matrix at position P' at the epoch of t_1 for the first pass; $\delta\mathbf{T}_{x^q}(\delta P)$ is the correction term for the gravity gradient matrix from the difference in location and attitude difference; $\delta\mathbf{T}_{x^q}^{t_{12}}(P)$ the correction term for the gravity gradient matrix from the change over the two months time; ε the noise in the observations.

In this thesis the correction term $\delta\mathbf{T}_{x^q}^{t_{12}}(P)$ is neglected, the noise ε between the two repeat tracks in the result is much higher than the time variation in the gravity field. Horizontal distance and altitude differences between one set ascending GOCE repeat tracks are plotted in Figure 4.6.

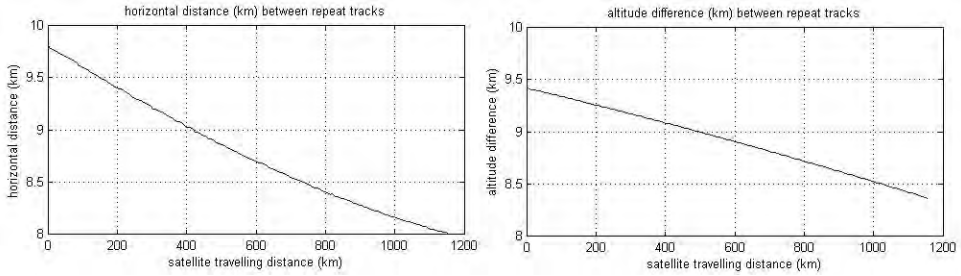

Figure 4.6: Repeat condition of one set GOCE repeat tracks

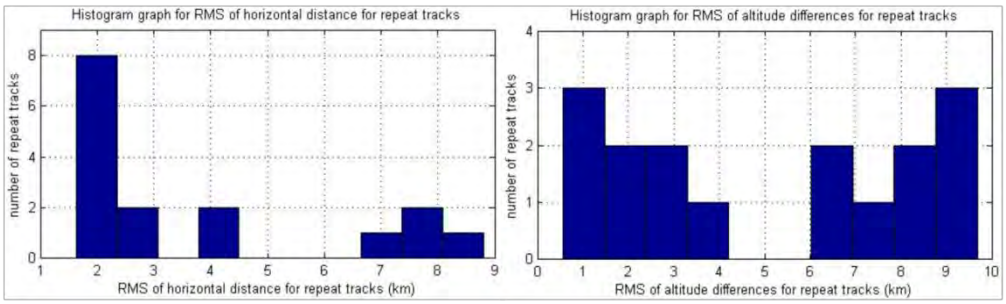

Figure 4.7: Histogram graphs of 16 repeat tracks condition

Between a set of two repeat tracks, the GOCE is not at the same altitude and also has a small difference in attitude. In Figure 4.6, the horizontal distance between the repeat tracks and altitude difference are shown. It is obvious that the repeat orbit cannot be exactly repeated. The objective of GOCE mission is providing the gravity field with 100 km spatial resolution, so 10 km difference is tolerable for our application. The histogram graphs of horizontal distances and altitude differences for 16 repeat tracks (Figure 4.10) are plotted in Figure 4.7. Horizontal distances between the repeat tracks are much lower than the altitude difference. RMS of horizontal distance for all repeat track, $RMS(D^{hor})$, is 3.8 km and RMS of altitude difference, $RMS(D^{r})$ is 5.0 km.

From section 2.3, the gravity gradient $\mathbf{T}$ from a global gravity model can be computed from the SH coefficients (S_{lm} and C_{lm}) and orbit altitude H. The SH coefficients are not available for the GOCE observations obviously, so we used the gravity gradient difference between repeat tracks positions from EGM2008 to correct the position and attitude mismatch. $\delta\mathbf{T}_{x^q}(\delta P)$ can be written as

$$\delta\mathbf{T}_{x^q}(\delta P) = \mathbf{T}_{x^q}^{t_2(ref.)}(P) - \mathbf{T}_{x^q}^{t_1(ref.)}(P'), \tag{4.5}$$

with superscript $^{(ref.)}$ the gravity gradient computed from a reference gravity model which is EGM2008 up to degree 300.

The correction terms $\delta\mathbf{T}^{x^q}(\delta P)$ for one pair of repeat tracks are shown in Figure 4.8. The radial gradient tensor correction term, $\delta\mathbf{T}_{zz}(\delta P)$, is larger than the other

two correction terms $\delta \mathbf{T}_{xx}(\delta P)$ and $\delta \mathbf{T}_{yy}(\delta P)$. The correction terms can reach up to 10 mE. The histogram graph for RMS of correction terms, $RMS(\delta \mathbf{T}_{x^q})$ is shown in Figure 4.9. The radial gradient $\delta \mathbf{T}_{zz}(\delta P)$ is larger than the other two correction terms. For all 16 pairs of repeat tracks $RMS(\delta \mathbf{T}_{xx})$, $RMS(\delta \mathbf{T}_{yy})$ and $RMS(\delta \mathbf{T}_{zz})$ are 1.8 mE, 1.5 mE and 2.9 mE, respectively.

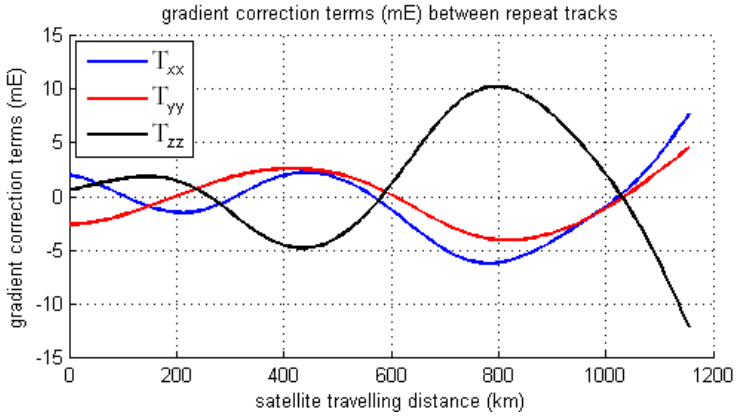

Figure 4.8: Gravity gradient correction terms from reference gravity model (EGM2008, up to degree 300)

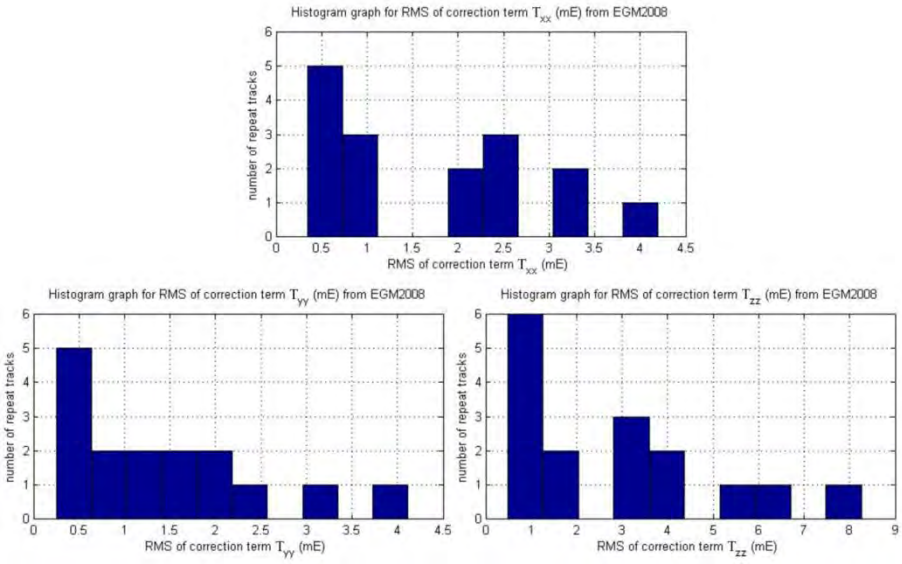

Figure 4.9: Histogram graph for RMS of correction terms derived from reference model (EGM2008, up to degree 300)

The flow chart of the repeat tracks comparison is showed in Figure 4.10. $\mathbf{T}^{ref.}$ is the gravity gradient matrix computed from the reference gravity model (EGM2008). $\mathbf{T}^{obs.}$ is the gravity gradient matrix from the GOCE level 2 product. $\overline{\mathbf{T}}^{ref.}$ and $\overline{\mathbf{T}}^{obs.}$ are the gravity gradient after the band-pass Butterworth filter with degree 10 from EGM2008 and GOCE, respectively. $\overline{\mathbf{T}}^{ref.}_{local}$ and $\overline{\mathbf{T}}^{obs.}_{local}$ are the filtered gravity gradients within the Reykjanes Ridge area.

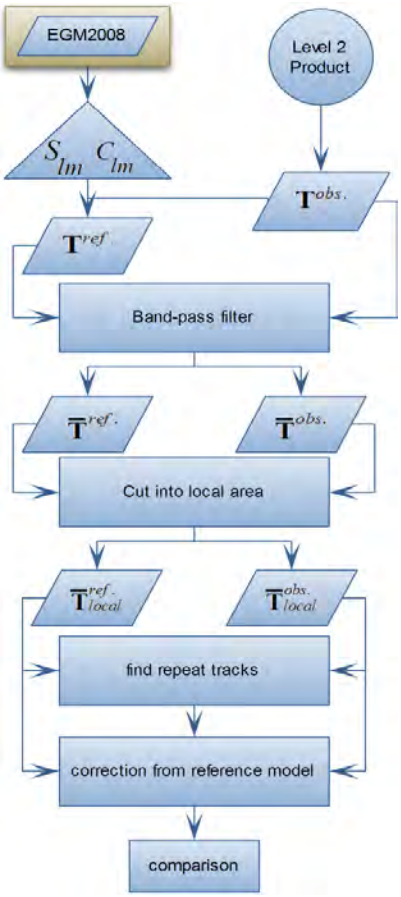

Figure 4.10: Flow chart of repeat tracks comparison

The result of the repeat track comparison is shown in Figure 4.11. The mean altitude difference between the GOCE track and the repeat track is about 9 km. The gravity gradients T_{xx} , T_{yy} and T_{zz} have no significant bias or trend differences between repeat tracks and nicely match the reference gravity model. The difference between the repeat tracks for T_{xx} is smaller than T_{yy} and T_{zz}, and T_{xx} has the best match to the reference model. The differences between the repeat tracks are mainly noise which might result from the imperfect band-pass filter as well as the noise in the gradiometer.

For all the GOCE orbit tracks plotted in Figure 4.5, the standard deviation of the difference of V_{zz} between GOCE observation and EGM2008, $STD(T_{zz}^{obs.} - T_{zz}^{ref.})$, and between repeat tracks , $STD(T_{zz}^{t_1} - T_{zz}^{t_2})$, are computed. $STD(T_{zz}^{obs.} - T_{zz}^{ref.})$ for all the tracks is 6.2 mE and $STD(T_{zz}^{t_1} - T_{zz}^{t_2})$ is 9.1 mE.

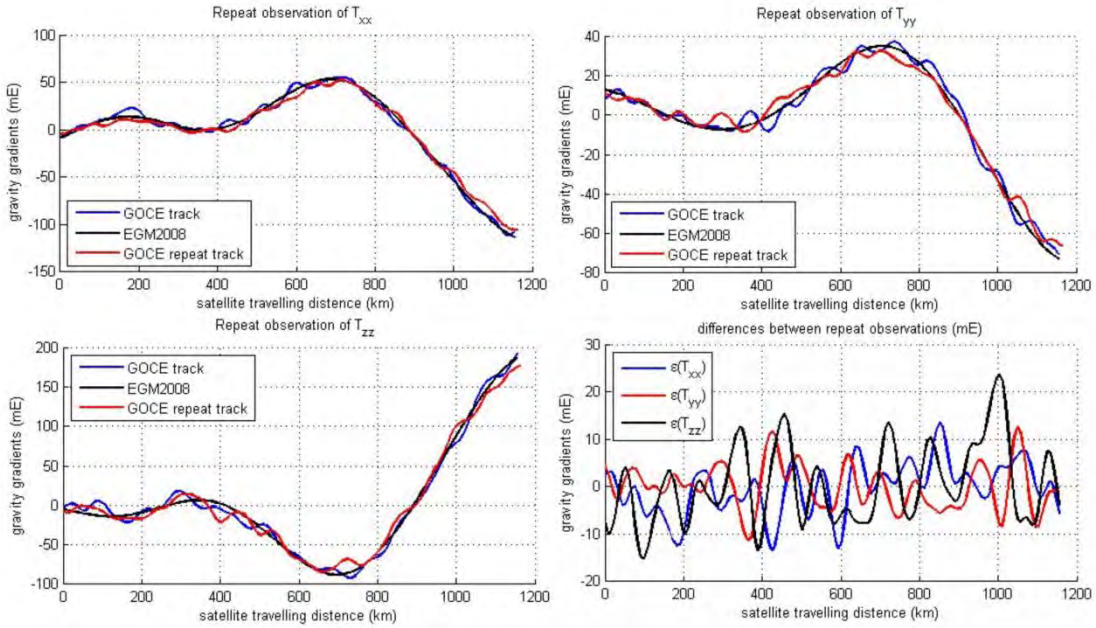

Figure 4.11: One set of repeat tracks comparison

The results from the repeat tracks comparison confirm the conclusions in Visser (2011) that GOCE filtered observations have a good consistency with the filtered gradients derived from global gravity field models. The standard deviation of the difference between the GOCE gradients and derived gradients in the local area around Reykjanes Ridge is 6.2 mE within the range of 3-7 mE from conclusion of Visser (2011), but larger than the 3 mE from Müller, et al. (2010) probably because no external calibration is applied in this thesis.

Chapter 5. Conclusions and recommendations

The GOCE mission provides for the first time satellite gravity gradient data. Implementation of a quality check before using the GOCE product is necessary. In this thesis, three GOCE gravity models (direct solution, space-wise solution and time-wise solution) and gravity gradients from GOCE Level 2 products are used for assessment. The external dataset used are the reference gravity models (ITG-Grace2010s and EGM2008), ship track measurements from NOAA and a simplified parametric geophysical model.

In the gravity models assessment, three GOCE gravity models compared to reference models (ITG-Grace2010s and EGM2008) globally and within the area of mid-Atlantic ridge (Reykjanes ridge). Compared to the state-of-the-art GRACE gravity field model ITG-Grace2010s which is derived from GRACE eight-year observations, significant improvements with respect to EGM2008 can be found for the three GOCE solutions which are computed from the two-month observations of GOCE mission. The direct solution shows improvement for degrees higher than 120, while the space-wise and time-wise solutions perform better than ITG-Grace2010s for degrees larger than 150.

Polar gaps affect GOCE time-wise solution more than other GOCE gravity models. The 6.5 degree polar gap strongly affects near zonal coefficients for the GOCE time-wise solution. Elimination of near zonal coefficients in spectral domain works better than elimination of polar area in spatial domain.

EGM2008 is not suitable for evaluating GOCE gravity field models for degrees from 70 to 150, as all the differences between the three GOCE solutions or ITG-Grace2010s and EGM2008 follow the same curve.

Three GOCE solutions show a better match to EGM2008 than ITG-Grace2010s after synthesizing up to degree 180. EGM2008 shows significant differences with respect to other gravity models in parts of Africa, South America and Himalayas. These are likely improvements found in GOCE solutions and ITG-Grace2010s.

A local comparison was done in an area containing part of mid-Atlantic ridge (Reykjanes ridge), south-west of Iceland, for comparison between three GOCE solutions and reference gravity models (EGM2008 and ITG-Grace2010s). A simplified parametric geophysical model is used for comparison. It was found that

a ridge center line derived from a topography map differs from the lines derived from the gravity field models. The ridge center lines derived from three GOCE solutions are almost straight lines. Geopotential undulations tracks match better in the southeast direction than northwest. Tracks synthesized from ITG-Grace2010s differ from the tracks synthesized from the other models.

In the local geoid comparison, differences of three GOCE solutions with respect to EGM2008 show a linear spatial pattern along the Greenland coastline. The linear spatial pattern appears within the observation wavelength of GOCE mission. EGM2008 contains several data sources, such as satellite altimetry on the coast with terrestrial data on land. The linear spatial pattern could result from the artificial patching of the satellite altimetry data and terrestrial data, or from the poorer quality of satellite altimetry near the coast than in the open ocean. GOCE mission can observe all locations on Earth except for areas close to the poles, thus it will have no problem to overcome continent-ocean boundaries.

After removing second order polynomial, ship tracks observation from NOAA are still too noisy for evaluating GOCE data in Reykjanes area. RMS differences for gravity at the location of the ship tracks derived from GOCE solutions with respect to adjusted ship tracks are slightly worse than tracks from ITG-Grace2010s.

In order to remove the signal outside of the measurement bandwidth of GOCE, a band-pass filter is required. After a discussion in Section 4.1, Butterworth band-pass filter with degree 10 is selected for along-track filtering of the Level 2 gravity gradients.

After filtering, the gravity gradients are compared within the Reykjanes area for the successive repeat tracks with location variation corrected. The level 2 GOCE gradients are close to the filtered gradients derived from EGM2008. For the selected 16 repeat tracks, the standard deviation between the filtered tracks level 2 GOCE gradients and tracks derived from EGM2008 is 6.2 mE which is close to the result of 3 mE from cross-over analysis by Müller, et al. (2010) who used external calibration with geopotential model. It also might result from the suboptimal filtering. The standard deviation between the pairs of repeat tracks of level 2 GOCE gradiens is 9.1 mE which suggests that the differences between the filtered GOCE gradient and gradients derived from EGM2008 are mainly noise.

A Ph.D candidate will continue this work in TU Delft. The filtering method should be improved for the gravity gradient assessment. Longer peoriod of GOCE gravity gradient measurement and larger area of interest are suggested for understanding the noise in the GOCE gradient measurements from the repeat track comparison.

References

Arabelos, D., & Tscherning, C. C. (1998). Calibration of satellite gradiometer data aided by ground gravity data. *Journal of Geodesy*(72), 617-625.

Bingham, R. J., Knudsen, P., Andersen, O., & Pail, R. (2011). An initial estimate of the North Atlantic steady‐state geostrophic circulation from GOCE. *Geophysical Research Letter, 38*(L01606).

Bouman, J., Bosch, W., & Sebera, J. (2011). Assessment of Systematic Errors in the Computation of Gravity Gradients from Satellite Altimeter Data. *Marine Geodesy, 34*(23), 85-107.

Bouman, J., & Koop, R. (2003). Error assessment of GOCE SGG data using along track interpolation. *Advances in Geosciences, 1*, 27-32.

Bouman, J., Koop, R., Sneeuw, N., & Tscherning, C. C. (2003). *Terrestrial Data for Calibration and Error Assessment of GOCE Gravity Gradients.* Paper presented at the Presented at EGS/EUG/AGU meeting 2003.

Bouman, J., Koop, R., Tscherning, C. C., & Visser, P. (2004). Calibration of GOCE SGG data using high-low SST, terrestrial gravity and global gravity field models. *Journal of Geodesy*, 124-137.

Bruinsma, S. L., Marty, J. C., Balmino, G., Biancale, R., Foerste, C., Abrikosov, O., & Neumayer, H. (2010). *GOCE gravity field recovery by means of the direct.* Paper presented at the ESA Living Planet Symposium, Bergen, Norway.

Butterworth, S. (1930). On the theory of filter amplifier. *Experimental Wireless & Wireless Engineering, 7*, 536-541.

Casotto, S., & Fantino, E. (2009). Gravitational gradients by tensor analysis with application to spherical coordinates. *Journal of Geodesy, 83*(7), 621-634. doi: 10.1007/s00190-008-0276-z

Champagne, B., Labeau, F., & Peter, K. (2004). Discrete Time Signal Processing.

ESA. (1999). Gravity Field and Steady-State Ocean Circulation Mission. Noordwijk, the Netherlands: ESA Publications Division.

ESA. (2006). GOCE L1b products user handbook.

ESA (Producer). (2009). Facts and figures. *European Space Agency*. Retrieved from http://www.esa.int/esaMI/GOCE/SEMDU2VHJCF_0.html

ESA (Producer). (2010a, May 26). ESA GOCE Mission Website. *GOCE mission overview*. Retrieved from http://www.esa.int/esaLP/SEMRNIRHKHF_LPgoce_0.html

ESA. (2010b). GOCE Level 2 Product Data Handbook.

ESA (Producer). (2010c, September 16). GOCE satellite. *European Space Agency*. Retrieved from http://www.esa.int/esaLP/ESA1MK1VMOC_LPgoce_2.html

ESA (Producer). (2011a, March 31). European Space Agency. *Earth's gravity revealed in unprecedented detail*. Retrieved from http://www.esa.int/esaEO/SEM1AK6UPLG_planet_0.html

ESA (Producer). (2011b). GOCE mission milestones. *European Space Agency*. Retrieved from http://www.esa.int/esaLP/ESABQK1VMOC_LPgoce_2.html

Foerste, C., Flechtner, F., Schmidt, R., Stubenvoll, R., & Rothacher, M. (2008). EIGEN-GL05C - A new global combined high-resolution GRACE-based gravity field model of the GFZ-GRGS cooperation. *Geophysical Research Abstracts, 10*(EGU2008-A-03426).

Gruber, T., Ackermann, C., Hosse, M., & Visser, P. N. (2010). *Validation of GOCE Gravity Field Models by Means of Geoid Comparisons and Orbit Fits.* Paper presented at the American Geophysical Union, Fall Meeting 2010, abstract #G31A-0796.

Haagmans, R., Prijatna, K., & Omang, O. (2002). *An alternative concept for validation of GOCE gradiometry results based on regional gravity.* Paper presented at the Gravity and Geoid 2002, Thessaloniki.

Heiskanen, W. A., & Moritz, H. (1967). *Physical Geodesy (reprint 1987)*. Graz: Institute of Physical Geodesy, Technical University Graz.

Hirt, C., Gruber, T., & Featherstone, W. E. (in press). Evaluation of the first GOCE static gravity field models using terrestrial gravity, vertical deflections and EGM2008 quasigeoid heights. *Journal of Geodesy*.

Ihde, J., Wilmes, H., Müller, J., Denker, H., Voigt, C., & Hosse, M. (2010). Validation of Satellite Gravity Field Models by Regional Terrestrial Data Sets. *System Earth via Geodetic-Geophysical Space Techniques*, 277-296.

Ilk, K. H. (1983). *Ein eitrag zur Dynamik ausgedehnter Körper: Gravitationswechselwirkung*. München: Deutsche Geodätische Kommission, Reihe C, Heft Nr.288.

Jeffreys, H. (1941). The Determination of the Earth'S Gravitational Field. *Geophysical Journal International, 5*, 1-22. doi: 10.1111/j.1365-246X.1941.tb00438.x

Johannessen, J. A., Balmino, G., Provost, C. L., Rummel, R., Sabadini, R., Sünkel, H., . . . Hughes, C. (2002). The European Gravity Field and Steady-State Ocean Circulation Explorer Satellite Mission Its Impact on Geophysics *Surveys in Geophysics*, 339-386.

Koop, R., & Stelpstra, D. (1989). On the computation of the gravitational

potential and its first and second order derivatives. *Manuscr Geod, 14*, 373-382.

Marsh, J. G., Lerch, F. J., Putney, B. H., Christodoulidis, D. C., Smith, D. E., Felsentreger, T. L., & Sanchez, B. V. (1988). A new gravitational model for the earth from satellite tracking data- GEM- T1. *Journal of Geophysical Research, 93*(B6), 6196-6215.

Mayer-Guerr, T., Kurtenbach, E., & Eicker, A. (Producer). (2010). ITG-Grace2010, Institut für Geodäsie und Geoinformation, Universität Bonn. Retrieved from http://www.igg.uni-bonn.de/apmg/index.php?id=itg-grace2010

Migliaccio, F., Reguzzoni, M., Sanso, F., Tscherning, C. C., & Veicherts, M. (2010). *GOCE data analysis: the space-wise approach and the first space-wise gravity field model.* Paper presented at the the ESA Living Planet Symposium, Bergen, Norway.

Moritz, H. (1989). *Advanced Physical Geodesy*. Karlsruhe: Wichman.

Müller, J., Denker, H., Jarecki, F., & Wolf, K. (2004). *Computation of calibration gradients and methods for in-orbit validation of gradiometric GOCE data.* Paper presented at the the 2nd Int. GOCE user workshop, Frascati.

Müller, J., Jarecki, F., Wolf, I., & Brieden, P. (2010). Quality Evaluation of GOCE Gradients,. *System Earth via Geodetic- Geophysical Space Techniques, Advanced Technologies in Earth Sciences*, 265-276.

Nerem, R. S., Jekeli, C., & Kaula, W. M. (1995). Gravity field determination and characteristics: Retrospective and prospective. *Journal of Geophysical Research, 100*(B8), 15,053-015,074.

NOAA. (2006). ETOPO2v2 Global Gridded 2-minute Database. *National Geophysical Data Center, National Oceanic and Atmospheric Administration*. Retrieved from http://www.ngdc.noaa.gov/mgg/global/etopo2.html

Novák, P., & Grafarend, E. (2006). The effect of topographical and atmospheric masses on spaceborne gravimetric and gradiometric data. *Studia Geophysica et Geodaetica, 50*(4), 549.

Oppenheim, A. V., & Shaffer, R. W. (1999). *Discrete-time Signal Processing*. New Jersey: Prentice-Hall.

Pail, R. (2002). In-orbit calibration and local gravity field continuation problem. Noordwijk: ESA

Pail, R., Goiginger, H., Mayrhofer, R., Schuh, W.-D., Brockmann, J. M., Krasbutter, I., . . . Fecher, T. (2010). *Global gravity field model derived from orbit and gradiometry data applying the time-wise method.* Paper presented at the ESA Living Planet, Bergen, Norway.

Pail, R., Goiginger, H., Schuh, W. D., Höck, E., Brockmann, J. M., Fecher, T., . . . Rieser, D. (2010). Combined satellite gravity field model GOCO01S derived from GOCE and GRACE. *Geophysical Research Letters, 37*(L20314).

Pail, R., & Plank, G. (2002). Assessment of three numerical solution strategies for gravity field recovery from GOCE satellite gravity gradiometry implemented on a parallel platform. *Journal of Geodesy, 76*(8), 462-472.

Pavlis, N. K., A.Holmes, S., Kenyon, S. C., & Factor, J. K. (2008). *An Earth gravitational model to degree 2160: EGM2008.* Paper presented at the European Geosciences Union General Assembly 2008, Vienna.

Reigber, C. (1989). Gravity field recovery from satellite tracking data. *Lecture Notes in Earth Sciences, Theory of Satellite Geodesy and Gravity Field Determination, 25*.

Reigber, C., Schwintzer, P., Neumayer, K.-H., Barhelmes, F., Koenig, R., Foerste, C., . . . Fayard, T. (2003). The CHAMP-only earth gravity field model EIGEN-2. *Advances in Space Research, 31*(8), 1883-1888.

Rummel, R., Balmino, G., Johanessen, J., Visser, P., & Woodworth, R. (2002). Dedicated Gravity Field Missions. Principles and Aims. *Journal of Geodynamics, 33*(1-2), 3-20.

Rummel, R., & Gruber, T. (2009). *GOCE Science Data Processing System Status and Plan.* Paper presented at the European Geosciences Union General Assembly 2009, Vienna.

Schuh, W. D. (2003). The processing of band-limited measurements; filtering techniques in the least squares context and in the presence of data gaps. *space science reviews, 108*(1-2), 67-78.

Seeber, G. (2003). *Satellite Geodesy (2nd Edt.)*. Berlin: Walter de Gruyter.

Sneeuw, N. (2006). Physical Geodesy. Stuttgart.

Sneeuw, N., & van Gelderen, M. (1997). The polar gap *Geodetic Boundary Value Problems in View of the One Centimeter Geoid, Lecture Notes in Earth Sciences* (Vol. 65, pp. 559-568). Berlin / Heidelberg: Springer.

Sünkel, H. (2001). *Europe's Preparation For GOCE Gravity Field Recovery.* Paper presented at the American Geophysical Union Fall Meeting 2001, San Francisco, USA.

Talwani, M., Windisch, C. C., & Langseth, M. G. (1971). Reykjanes Ridge Crest: A Detailed Geophysical Study,. *Journal of Geophysical Research, 76*, 473-577.

Tscherning, C. C. (1976). Covariance expressions for second and lower order derivatives of the anomalous potential. Colombus.

Turcotte, D. L., & Schubert, G. (2002). *Geodynamics*. New York: Cambridge University Press.

Visser, P. N. A. M. (2011). A glimpse at the GOCE satellite gravity gradient observations. *Advances in Space Research, 47*(3).

Wahr, J., Molenaar, M., & Bryan, F. (1998). Time variability of the Earth's gravity field: Hydrological and oceanic effects and their possible detection using GRACE. *journal of geophysical research, 103*(B12), 30205-30229.